Advances in Water Resources 159 (2022) 104093

Contents lists available at ScienceDirect

Advances in Water Resources

journal homepage: www.elsevier.com/locate/advwatres

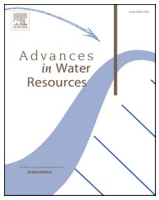

Assessing the potential value of the regionalised input constraint indices for constraining hydrological model simulations in the Congo River Basin

Pierre M. Kabuya [a,e,*], Denis A. Hughes [a], Raphael M. Tshimanga [b,e], Mark A. Trigg [c], Paul Bates [d]

[a] Institute for Water Research, Rhodes University, Box 94, Grahamstown 6140, South Africa
[b] Congo River Basin Water Resources Research Center (CRREBaC), University of Kinshasa, Kinshasa, DRCongo
[c] School of Civil Engineering, University of Leeds, Leeds, Northern Ireland LS2 9JT United Kingdom
[d] School of Geographical Sciences, University of Bristol, Bristol, Northern Ireland BS8 1SS, United Kingdom
[e] Department of Natural Resources Management, Faculty of Agronomic Sciences, University of Kinshasa, Lemba Kinshasa, DRC, PO Box 127 Kinshasa XI.

ARTICLE INFO

Keywords:
Uncertainty
Constraints
Modeling
Pitman model
Congo Basin

ABSTRACT

The regionalised characteristics of a sub-basin's long-term hydrological behaviour are used as multiple constraint filters for constraining hydrological model simulations in the Congo Basin using the monthly time step Pitman model. The results suggest that the constraints are appropriate in many sub-basins ($\geq$ 20 gauging stations), but not all. Detailed examination of these results suggested that the effects of high slopes ($>$ 7%) could increase the runoff ratio and Q90/MMQ (low flow index) constraint values and that implementing an adjustment factor based on slope did improve some of the very poor results. The percentage points on the FDC falling within the simulated uncertainty band has increased from 0% to 59.6% and 2.4% to 39.9% for the Rift valley and Batéké plateaux regions, respectively. Future studies ideally need a range of different rainfall products to quantify the uncertainties related to the inappropriateness of the CRU rainfall data in some parts of the Congo Basin.

1. Introduction

Adequate quantification of hydrological information across different spatial and temporal scales is essential to ensure sustainable management of water resources (Quesada-Montano et al., 2018). Hydrological models are used to generate such information (Fleischmann et al., 2018). However, the limitations of the available observed streamflow records (short records, missing data and lack of spatial representativeness), typical of data-scarce regions, limit the use of traditional model calibration and validation approaches and contribute to increased uncertainty in the estimation of water resources. In many large river basins (including the Congo River Basin), many of the available streamflow gauging stations are located in the downstream parts of the basin and represent cumulative streamflow characteristics from relatively large catchment areas. The data are therefore not very useful for quantifying regional patterns of response in headwater areas (Kabuya et al., 2020b). This presents a serious limitation to hydrological modelling and makes it difficult to quantify model behavioural parameters (those generating hydrological responses that match observed conditions) for the individual upstream sub-basins (Hughes, 2016). It is, therefore, necessary to resort to hydrological modelling approaches that can realistically quantify the uncertainty associated with water resources estimations (Ndzabandzaba and Hughes, 2017; Quesada-Montano et al., 2018). However, this also means that water resources decision-making processes have to allow for this uncertainty (McMillan et al., 2017; Hughes, 2019).

Although the Congo River Basin appears to be less studied than other large river basins of the world such as the Amazon (Alsdorf et al., 2016; Laraque et al., 2020), some published studies have tackled different aspects of hydrological research. Amongst the available studies, relatively few have focused on the use of rainfall-runoff models (Chishugi and Alemaw, 2009; Beighley et al., 2011; Tshimanga et al., 2011; Tshimanga and Hughes, 2014; Aloysius and Saiers, 2017; Munzimi et al., 2019) of different complexities, for either process understanding, present-day water resource availability, or future climate change impact assessment. A common issue arising from the application of these models in the Congo Basin is the multiple uncertainty sources associated with the simulated hydrological response. For example, studies by Beighley et al. (2011) and Aloysius and Saiers (2017) reveal that the lack of a large and spatially extensive dataset at the appropriate scales can

* Corresponding author at: Department of Natural Resources Management, Faculty of Agronomic Sciences, University of Kinshasa, Lemba Kinshasa, DRC, PO Box 127 Kinshasa XI.
E-mail address: kabuyabal@gmail.com (P.M. Kabuya).

https://doi.org/10.1016/j.advwatres.2021.104093
Received 17 August 2021; Received in revised form 3 November 2021; Accepted 25 November 2021
Available online 28 November 2021

result in very high uncertainty. They used a basin physiographic dataset in an *a priori* parameter estimation approach. However, the coarse resolution of the physiographic datasets that were not initially produced for hydrological applications are considered to remain as a main source of uncertainty in hydrological modelling. O'Loughlin et al. (2019) reported that the simulated daily discharges from Beighley et al. (2011) required bias-correction before being used as input to a hydrodynamic model. Tshimanga and Hughes (2014) identified the primary sources of uncertainty in the application of a monthly time-step hydrological model in the Congo River Basin and recommended the use of regionalised hydrological indices (or the characteristics of a sub-basin's long-term hydrological behaviour) to overcome some of the problems of data scarcity. These few examples show that uncertainty will always be present in hydrological simulations (Beven, 2006; Hughes, 2016). Uncertainties in water resources estimation can be caused by climate inputs (McMillan et al., 2012; Westerberg and Mcmillan, 2015; Ehlers et al., 2019), streamflow discharge data (Westerberg et al., 2011b; McMahon and Peel, 2019), model structure (Gupta and Govindaraju, 2019), and model parameters (Mehdi et al., 2018). Other uncertainty sources include the shortness of available streamflow series and a poor representation of the long-term flow regime (Westerberg et al., 2014), lack of spatial representation, making it difficult to interpolate to ungauged sub-basins, undocumented upstream water development infrastructure and the effects of large wetland areas (Tshimanga and Hughes, 2014; Tumbo and Hughes, 2015; Ndzabandzaba and Hughes, 2017).

Methods that quantify the uncertainty directly from the streamflow data are based on either discharge gaugings themselves (Coxon et al., 2015), stage gaugings (McMillan et al., 2012; Horner et al., 2018) or rating-curve uncertainty (Westerberg and McMillan, 2015). Kiang et al. (2018) and McMahon and Peel (2019) reviewed some of these methods. However, their application in the context of the Congo Basin is difficult, due to the small amount of streamflow data. In the Congo Basin, technical information on rating curves and associated uncertainty are not often available (Tshimanga and Hughes, 2014). This makes it impractical to quantify uncertainty from individual data sources, and alternative methods are required to realistically quantify the total uncertainty associated with hydrological estimates. These alternatives include the use of regionalised hydrological indices to constrain hydrological model simulation uncertainties. Previously, such approaches were focused on the limits of acceptability based on flow duration curves (FDCs) (Beven, 2006; Blazkova and Beven, 2009; Westerberg et al., 2011a; Beven, 2012; Beven and Binley, 2014; Teweldebrhan et al., 2018) and later evolved to include additional signatures to reflect different water balance components (Yadav et al., 2007; Zhang et al., 2008; Westerberg and Mcmillan, 2015; Shafii and Tolson, 2015; Almeida et al., 2016; Ndzabandzaba and Hughes, 2017; Nijzink et al., 2018). Such methods have the advantage of assessing the limits of model acceptability (uncertainty), rather than normal methods of measuring reliability (such as objective functions based on comparisons with the measured data) (Westerberg et al., 2011a; Beven, 2012). The limits (or constraints) on model acceptability are also model independent.

Two studies (Tumbo and Hughes, 2015; Ndzabandzaba and Hughes, 2017) conducted in the southern Africa region used six hydrological indices representing the main water balance components. These six indices were used to constrain the Pitman model outputs and establish appropriate (behavioural) parameter sets. The parameter sets that generated simulations that met all of the constraint ranges were referred to as behavioural. Quesada-Montano et al. (2018) used four different constraints based on climate and runoff process characteristics at different time-scales to reject HBV-light model parameters that failed to represent hydrological process characteristics of a Costa Rican catchment. Nijzink et al. (2018) constrained the feasible parameter space of conceptual hydrological models using different remote sensing products of soil moisture, evaporation, and total water storage and snow accumulation for 27 catchments across Europe.

Yadav et al. (2007) developed prediction limits of hydrological constraint indices with associated confidence intervals for 30 UK catchments. Such limits were used by both Yadav et al. (2007) and Kapangaziwiri et al. (2012) to define regional constraint uncertainty. Similarly, Ndzabandzaba and Hughes (2017) applied uncertainty bounds around previous simulations to define the constraint ranges and developed regional relationships between the aridity index (ratio of the mean annual potential evapotranspiration and the mean annual rainfall) and hydrological indices for Eswatini (formerly Swaziland). In contrast, Quesada-Montano et al. (2018) applied a subjective ±20% uncertainty to the runoff ratio inspired by uncertainty studies conducted elsewhere (Westerberg and Mcmillan, 2015). In another study by Tumbo and Hughes (2015) where it was difficult to find regional patterns in the relationships between sub-basin physical attributes and the hydrological indices, the constraint ranges were based on simple index ranges for each identified region in the Great Ruaha River basin of Tanzania. These few examples highlight the need for extracting the most possible information from the available data to define realistic constraint ranges in the context of ungauged basins (Hrachowitz et al., 2013).

In the Congo Basin, the initial study by Tshimanga and Hughes (2014) used an *a priori* estimation approach to estimate uncertainty ranges for the Pitman model parameters. While the simulations were generally acceptable, there remained some unresolved uncertainty issues, partly due to the coarse resolution of the physical basin properties used to set the parameter ranges. Kabuya et al. (2020b) developed uncertainty ranges of some hydrological indices across different climate and physiographic regions of the Congo River Basin using confidence intervals of the predictive equations based on the aridity index. The present study builds on the latter (Kabuya et al., 2020b) and mainly aims at testing the applicability of these index ranges in constraining the simulation uncertainties of a hydrological model of the Congo River Basin. Specifically, the paper is focussed on applying the constraints for simulations using the Pitman model and evaluating the results using the same set of sub-basins (mainly headwater areas) used to develop the regional relationships, as well as additional gauged data located downstream of groups of sub-basins (the validation data). The overall objective is to assess the potential value of the approach for constraining hydrological model simulations in all the defined sub-basins of the Congo River Basin, and to identify where the likely methodological gaps are and how they might be filled.

2. Study area and available data

The climate of the Congo River Basin is warm and humid with two distinct wet and dry seasons that vary with distance from the equator (Bultot, 1974; Samba et al., 2008). Land cover varies from tropical evergreen forest, with little seasonal variation, in the central parts, to savannah in the north and south (Mayaux et al., 2000; Hansen et al., 2008). Forest constitutes the primary land cover with an area of $\sim 2.3 \times 10^6$ km^2, representing about 18% of the world's tropical forests (Hansen et al., 2008; Somorin et al., 2012), and placing the Congo Basin second in the world after only the Amazon.

A total of 403 sub-basins have been delineated in the Congo River Basin (Tshimanga et al., 2020) and there are a total of 58 streamflow gauging stations (Kabuya et al., 2020b). The monthly streamflow time series (Fig. 1b and Table 1), were obtained from several sources including: the Global Runoff Data Centre (Fekete et al., 1999), the Office National de Recherche et du Developpement (Lempicka, 1971), Hydrosciences Montpellier—Système d'Informations Environnementales (SIEREM, http://hydrosciences.fr/sierem) and the Annuaire hydrologique du Congo Belge (Devroey, 1951). Some of the gauges are on the main river or its main tributaries and represent a large number of upstream sub-basins, while others are affected by upstream large wetland systems. These are not used in this study as it would be difficult to resolve either the upstream heterogeneity or the wetland impacts. Of the remaining 31 gauges, 9 represent headwater sub-basins, or groups of no more than 6 upstream sub-basins (7) and were used to develop initial

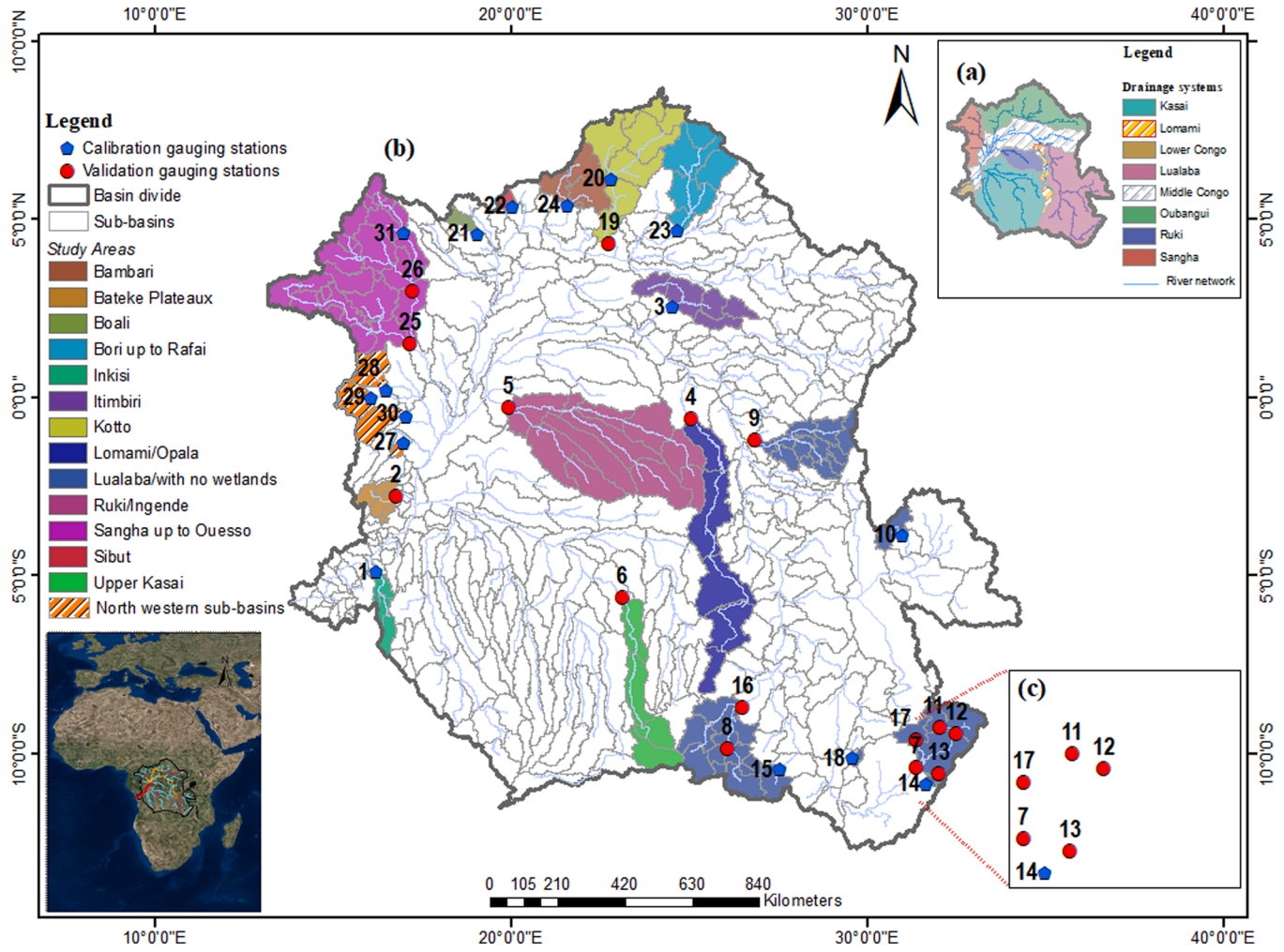

Fig. 1. The Congo River Basin and its major drainage systems showing the 16 gauges (blue dots) used in the previous study of Kabuya et al. (2020b) and the additional 15 gauges (red dots) used for validation (the inset shows the headwater gauges in the upper Lualaba system). Refer to Table 1 for the gauge names.

regional hydrological index constraint ranges (indicated by blue symbols in Fig. 1b), based on relationships with the aridity index (Kabuya et al., 2020b). These indices consisted of mean monthly flow volume (MMQ) and three non-dimensional flow duration curve indices (FDC10/MMQ, FDC50/MMQ and FDC90/MMQ). The remaining 15 gauges represent some headwater sub-basins (5) or groups of sub-basins and these are used as the validation set in this study (indicated by red symbols in Fig. 1). Table 1 lists the stations used in this study, while Table 2 lists only the non-headwater gauges and the number of upstream sub-basins.

The monthly rainfall forcing data used for the model are the Climate Research Unit (CRU TS 3.10) data for the period of 1901 to 2014 (Harris et al., 2014), at a spatial resolution of 0.5°. The UNIDEL (University of Delaware) rainfall dataset (covering the same period and spatial resolution) was used to check the appropriateness of the CRU rainfall data in specific areas (Sun et al., 2018). The CRU rainfall data have previously been successfully used for hydrological modelling in the Congo Basin (Tshimanga and Hughes, 2014). However, while gridded rainfall data might represent the general characteristics of the real rainfall (i.e. seasonality and frequency characteristics), they may not represent individual months very well. The monthly distributions of potential evapotranspiration (PET) required by the model are derived from the International Water Management Institute website (http://www.iwmi.org) and have been computed using climate information derived from New et al. (2002) for the period between 1961 and 1990. These climate data are used to calculate the aridity index using annual means of PET/Rainfall. Also, the daily (MOD16A2.006) MODIS actual evapotranspiration (AET) estimates (Running et al., 2017) with a spatial resolution of 500 m x 500 m, aggregated by year, were used to detect potential uncertainties in some of the long-term water balance components (stream flow = rainfall - evaporative losses). These global climate datasets are used given the lack of adequate ground-based information available for long periods and with good spatial coverage. However, the paucity of rainfall gauges over the Congo River Basin means that only limited observed records are used to construct and validate the global datasets, contributing a source of input uncertainty that cannot be readily quantified (Tshimanga, 2012; Maidment et al., 2015; Sun et al., 2018). Mean monthly recharge (MMR mm) index values are available from the global database of annual long-term average groundwater recharge (Döll and Fiedler, 2008) at a spatial resolution of 0.5° by 0.5° (Fig. 2), but are expected to be very uncertain in the absence of any observed measurements across the basin.

3. Materials and methods

3.1. Hydrological model

Arguably any single model, or group of models, could be used to achieve the stated objective of evaluating the usefulness of the regional hydrological indices for constraining the model(s) outputs, largely because the general approach is model independent. In this study, the monthly time step Pitman model (Pitman, 1973; Hughes, 2013) has been

Table 1
Streamflow gauging stations with different periods of records across different drainage systems of the Congo Basin (the stations included in the original regionalisation of hydrological indices are highlighted in bold).

SN	Sub-basin code	Long.	Lat.	Drainage area (km^2)	Station Name	Period of record	% missing Months
1	**C_CB138**	15.07	−5.13	12 824	Inkisi	1950–1959	22.5
2	C_CB169	15.65	−2.90	12 295	Bwambe	1951–1994	19.3
3	**C_CB185**	23.78	2.75	35 056	Itimbiri/Aketi	1950–1959	0.0
4	C_CB188	24.35	−0.60	91 396	Opala	1950–1959	0.0
5	C_CB218	18.94	−0.27	167 229	Ingende	1951–1959	10.1
6	K_CB259	22.31	−5.90	46 336	Kananga-L.	1952–1970	0.9
7	L_CB18	31.07	−10.95	34 745	Old Pontoon	1972–2004	20.7
8	L_CB27	25.41	−10.43	17 927	Nzilo	1921–1938	0.0
9	L_CB191	26.23	−1.24	42 322	Yumbi	1952–1959	1.1
10	**L_CB196**	30.57	−4.04	8 395	Taragi	1971–1979	5.6
11	L_CB200	31.7	−9.78	4 666	Chandawayaya	1978–1981	2.7
12	L_CB201	32.16	−10.00	16 572	Mbesuma P.	1974–2004	29.5
13	L_CB202	31.60	−11.20	1 008	Shiwa Ngandu	1964–1992	10.4
14	**L_CB203**	31.28	−11.49	1 147	Chikakala	1970–2004	17.9
15	**L_CB205**	26.95	−11.04	8 586	Kapolowe	1933–1959	7.4
16	L_CB207	25.86	−9.19	61 385	Bukama	1933–1959	11.1
17	L_CB230	30.96	−10.18	6 366	Kasama	1969–2006	2.4
18	**L_CB261**	29.09	−10.71	1 321	Chipili	1971–1981	0.8
19	O_CB76	21.92	4.61	77 924	Kembe	1954–1978	9.7
20	**O_CB95**	22.00	6.56	60 685	Bria	1954–1978	9.7
21	**O_CB176**	18.03	4.91	4 793	Boali	1949–1988	48.9
22	**O_CB179**	19.08	5.73	2 538	Sibut	1951–1991	45.1
23	**O_CB181**	23.94	5.01	52 527	Rafai	1952–1973	16.1
24	**O_CB355**	20.67	5.78	29 851	Bambari	1952–1975	21.3
25	S_CB55	16.07	1.62	158 284	Ouesso	1959–1983	0.0
26	S_CB61	16.12	3.20	71 424	Salo	1953–1994	35.0
27	**S_CB134**	15.85	-1.28	1 866	Komo Olombo	1963–1975	0.1
28	**S_CB158**	15.45	0.36	11 686	Yengo	1961–1980	0.3
29	**S_CB236**	14.92	0.05	10 492	Etoumbi	1951–1971	0.3
30	**S_CB243**	15.96	-0.5	1 159	Kouyou a linnegue	1953–1970	0.3
31	**S_CB395**	15.86	4.94	18 559	Carnot	1954–1971	19.9

Table 2
Sub-basins representing the non-headwater gauges with the number of upstream sub-basins (the stations included in the original regionalisation of hydrological indices are highlighted in bold).

SN	Sub-basin code	Total no. of upstream sub-basins	Upstream gauges
1	**C_CB138**	3	
2	C_CB169	4	
3	**C_CB185**	5	
4	C_CB188	5	
5	C_CB218	10	
6	K_CB259	4	
7	L_CB18	4	L_CB200, L_CB201, L_CB202
8	L_CB27	3	
9	L_CB191	12	
10	**L_CB201**	2	L_CB200
11	L_CB207	10	L_CB27
12	O_CB76	8	O_CB95
13	**O_CB95**	6	
14	**O_CB176**	3	
15	**O_CB181**	5	
16	S_CB55	24	S_CB61, S_CB395
17	S_CB61	12	S_CB395
18	**S_CB236**	2	
19	**S_CB395**	6	

used for two main reasons. The first main reason is that it has been previously applied successfully in many parts of the southern Africa region, including the Congo River Basin itself (Kapangaziwiri et al., 2012; Hughes, 2013; Tshimanga and Hughes, 2014; Tumbo and Hughes, 2015; Ndzabandzaba and Hughes, 2017; Oosthuizen et al., 2018; Kabuya, 2020). Further applications therefore build on the existing experience base of the model, while that same experience base is helpful for establishing likely model parameter values. The second main reason is that the model is packaged with a freely available model application interface (SPATSIM: https://www.ru.ac.za/iwr/research/software/spatsim/) that allows the model to be run in different ways that are appropriate to this study (see below for more details). SPATSIM consists of a variety of tools to store and manage the required data, as well as set up and run the model and analyse the outputs. This is not only valuable for this study, but also benefits other potential users in the region who may wish to replicate and expand on this study, or apply similar methods in other areas, but who may not have access to the necessary software development tools or skills to adapt a different model.

The model consists of storages (interception, soil moisture and groundwater) linked by functions to explicity represent the main runoff generation processes (infiltration excess, saturation excess and direct overland flow, interflow and groundwater flow) considered to occur at the sub-basin scale. Fig. 3 illustrates the model structure, while a brief description of the model parameters is given in Table 3. The model components and associated parameters are explained in more detail in previous publications (Hughes et al., 2006; Hughes, 2013; Tumbo and Hughes, 2015; Hughes and Mazibuko, 2018), while a quite comprehensive guide is available on the website (https://www.ru.ac.za/iwr/research/software/). There is little doubt that the model has a relatively high number of parameters, and a high level of equifinality, compared to many more parsimonious models (Beven, 2006; Hughes, 2016; Quesada-Montano et al., 2018; Her and Seong, 2018). However, in the context of this study, this is not considered to be a limiting issue, because the model outputs are constrained by the regionalised indices of hydrological behaviour and strictly speaking not based on any specific method of parameter calibration.

There are four main versions of the model as illustrated in Fig. 4. The first (V1) is a simple single-run version that uses a single climate input and parameter set to generate a single simulation for each sub-basin. This is largely used for manual calibration of the model and was not used in this study. The second (V2) represents stage 1 of a two stage uncertainty approach (Tumbo and Hughes, 2015; Ndzabandzaba and

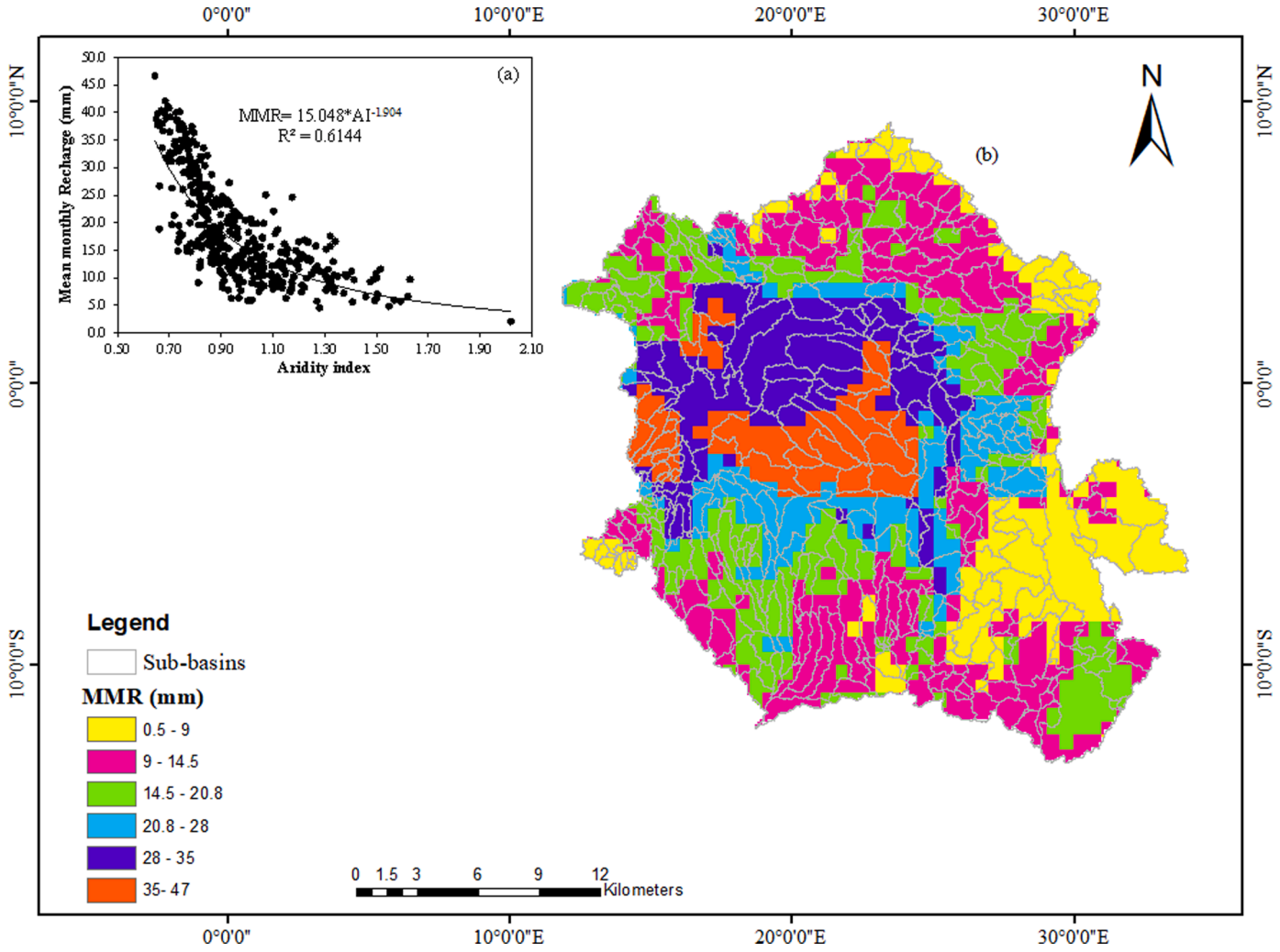

Fig. 2. Estimates of the uncertainty range of groundwater recharge across the Congo Basin. The inset shows the relationship between the mean recharge and the aridity index.

Hughes, 2017). The first stage simulates incremental flow contributions from one or more sub-basins independently (i.e. no cumulative flow routing). The parameter inputs consist of ranges of values for any parameters that are considered uncertain, while the uncertainty ranges of a set of hydrological indices also form part of the input. The model is run many times (with a user selectable option of 10 000, 50 000 or 100 000), with all the parameter values being randomly sampled from their ranges (i.e. assuming a uniform distribution). If any single model run generates a simulation that has characteristics falling within all of the ranges of a set of hydrological indices ('multiple constraint filters' in Fig. 4, namely the mean monthly runoff volume (MMQ in m^3 *10^6), mean monthly groundwater recharge depth (MMR in mm), the 10th, 50th and 90th percentiles of the flow duration curve expressed as a fraction of MMQ (Q10/MMQ, Q50/MMQ, Q90/MMQ) and the percentage of time that zero flows are expected), then it is accepted as behavioural and the parameter set is saved for later use in stage 2 (V3B). The model run stops when the user-defined number of behavioural parameter sets has been generated. The key issue is that not only must the constraint indices be compatible with each other (e.g. flow duration curve 90th percentile must be compatible with the groundwater recharge constraint), but the input parameter ranges must also be compatible with the constraint index ranges (e.g. the groundwater parameters should be compatible with the groundwater recharge constraint index range). There are built in facilities to guide users in the 'calibration' of the input parameter ranges to ensure that they are appropriately compatible and to ensure the efficient achievement of the required number of behavioural ensemble outputs, given the specified total number of possible model runs.

The third version of the model runs the model many times (typically 10 000) for the whole basin to generate cumulative flows at each sub-basin outlet. This can be based on independent random sampling of the input parameter ranges (V3A; unconstrained uncertainty assessment), or it can be based on re-sampling the complete parameter sets that were saved during the stage 1 model runs referred to above (V3B; constrained uncertainty assessment). In both cases, if there are observed data available, the outputs include a range of objective functions that can be used to evaluate individual ensemble members against the available observed data. The former can be useful to explore parameter equifinality and sensitivity (Hughes and Farinosi, 2021), while the latter represents the second stage of the 2 stage uncertainty approach based on hydrological index constraints. Both of these options have been used in this study.

The final version is similar to the third, except that the input rainfall data consists of ensembles rather than a single time series. Each rainfall input (typically 500) is used in combination with either unconstrained (V4A) or constrained (V4B) parameter sampling, to generate simulated flow ensembles that represent a combination of climate and parameter uncertainty. This version has been used in climate change assessments (Hughes and Farinosi, 2020), but is not used in this study.

These model versions are well suited for the Congo Basin because it is

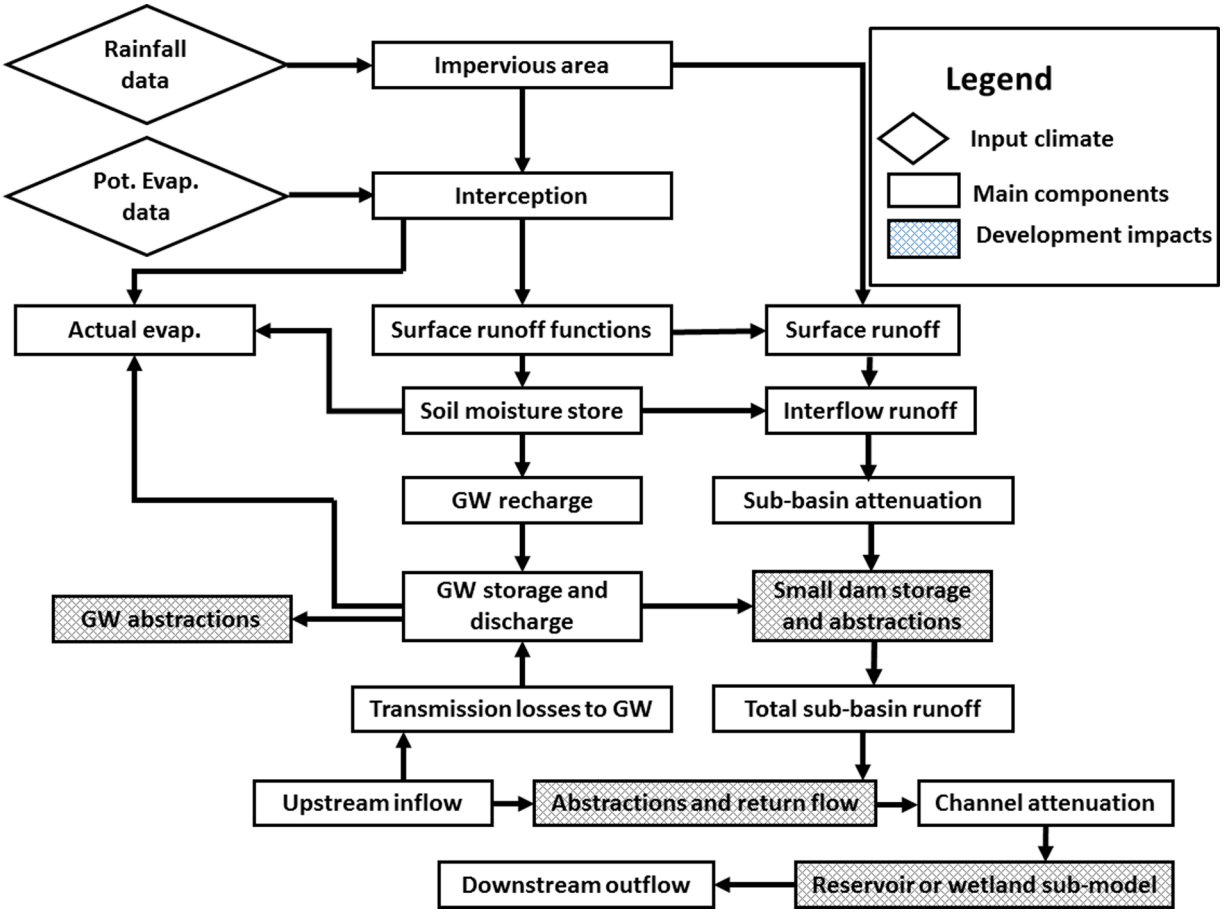

Fig. 3. Structure of the Pitman model with its main components.

Table 3
Description of the Pitman model main parameters (note that the model outputs are not very sensitive to some parameter value changes and these are frequently used with fixed values).

Model Parameter	Description	Units
RDF	Rain Distribution factor	[-]
PI1 and PI2	Interception storage for two types of vegetation	mm
AFOR	The proportion of the basin area covered by the second vegetation type	%
FF	The ratio of forest/grassland potential evapotranspiration	[-]
SER	Fraction of ST at which saturation excess runoff is initiated	[-]
PEVAP	Annual sub-basin Evaporation	mm
ZMIN, ZAVE, ZMAX	Minimum, average and maximum soil absorption rate for each sub-basin	mm month^{-1}
ST	Maximum moisture storage capacity	mm
FT	Runoff from moisture storage-runoff equation	mm month^{-1}
POW	Power of the moisture storage-runoff equation	[-]
GW	Maximum groundwater recharge at moisture storage full capacity	mm month^{-1}
GPOW	Power of moisture storage - groundwater recharge equation	[-]
R	Evaporation-moisture storage relationship	[-]
CL	Channel routing coefficient	Months
TL	Lag of surface and soil moisture runoff	Months
DDENS	Drainage density	km/km^{-2}
T	Groundwater transmissivity	m^2 day^{-1}
S	Groundwater storativity	[-]
RGWS	Initial groundwater drainage slope	%
GWL	Rest water level (m below surface)	m
RSF	Riparian Strip Factor	%

known as one of the most ungauged tropical basins where the majority of the available gauging stations reflect cumulative flow characteristics, making it difficult to distinguish the incremental flow contributions from different upstream sub-drainage systems. Through the regionalised hydrological indices, it is possible to identify behavioural parameters that reflect the sub-basin's incremental flow contributions. The model also provides the possibility of accounting for a sub-basin's development conditions such as water abstraction (e.g. reservoirs) and different types of regulations (e.g. hydropower dams), in the stage 2 (V3B) of the modelling approach. In addition, the general model structure (Fig. 3) provides a function that deals with wetlands where they are expected to exert considerable impacts on downstream flow regime.

3.2. Steps in the analysis

In an iterative process, Kabuya et al. (2020b) identified the aridity index as the main predictor of the hydrological response across the basin. The authors used climate and physiographic attributes (topographic wetness index, slope, fractions of silt, sand, clay and curve number) that are known to have potential relationships with sub-basin hydrological response characteristics (Buchanan et al., 2014; Beck et al., 2015; Zeng et al., 2017). They indicated that due to the scarcity of available headwater gauging stations, it was impractical to develop predictive equations of the hydrological response for each identified physiographic region of the Congo Basin. Therefore, the alternative approach of developing generic predictive equations for the whole basin was adopted with the aridity index producing the best results for all of the hydrological indices used. However, the authors did expect that this would pose some problems in areas where there may be additional factors apart from the aridity index that determine differences in

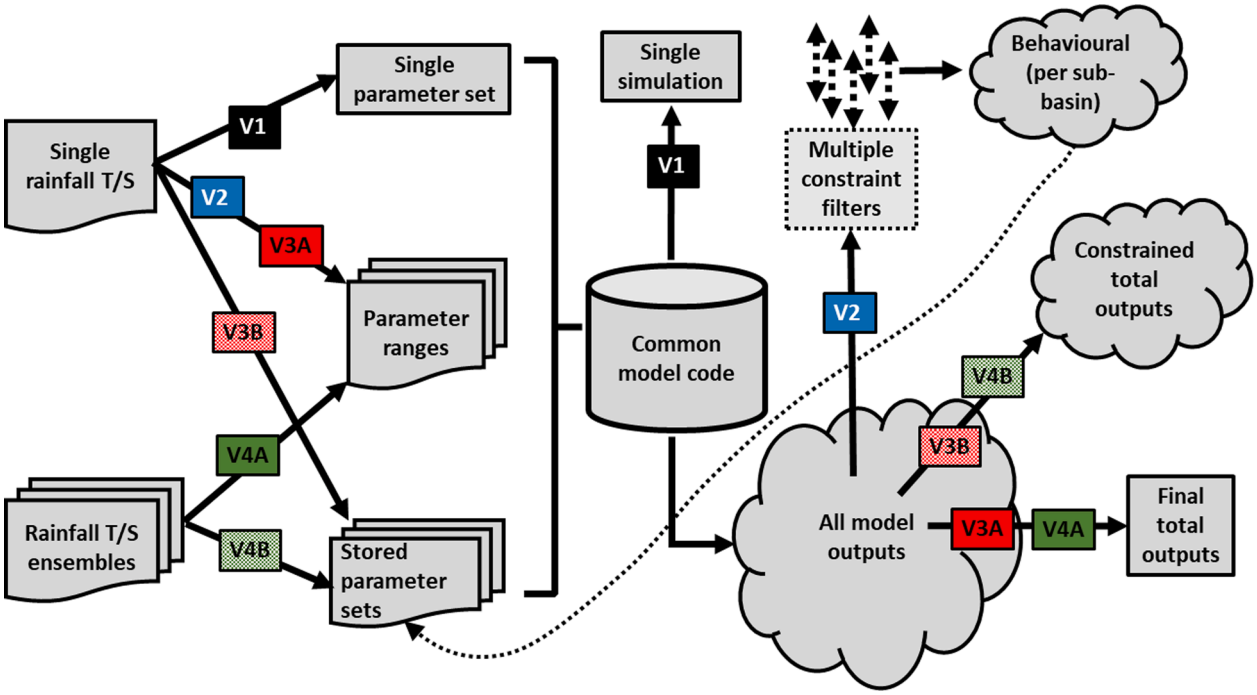

Fig. 4. Flow diagram illustrating the structure of the different methods (model versions) of using the Pitman model available with the SPATSIM framework.

hydrological response (Kabuya et al., 2020b). This challenge and others related to the temporal scaling of the constraints and identified convergence of the uncertainty bounds at low aridity index values are addressed in this analysis.

3.2.1. Step 1: temporal scaling of the constraints

It is possible that the streamflow constraint indices are not independent of the time period being simulated. Kabuya et al. (2020b) indicated that while every attempt was made to adopt a similar period for all the gauges used in the regional analysis of hydrological indices, the large differences between the gauges used and the lack of suitable adjacent stations available to extend the series, means that quite different periods were used in some cases. Therefore, the initial step in the assessment analysis is to re-calculate the hydrological index range for the common simulation period used in this study (1901 to 2014). This involved using the unconstrained uncertainty model version (V3A; Fig. 4) and finding the ensemble that most closely matches the observed streamflow data for the common overlap period. The hydrological indices (MMQ, Q10/MMQ, Q50/MMQ and Q90/MMQ) were then calculated for the selected ensemble for the overlap period and for the total period and checked to identify if there were any significant differences.

3.2.2. Step 2: critical analysis of the constraint predictive equations

The uncertainty bounds that were reported in Kabuya et al. (2020b; Fig. 11) were based on fitting power relationships to the 5% and 95% confidence intervals around the regression relationships. However, it was subsequently noted that for both MMQ and Q90/MMQ the lower and upper bounds started to converge at low aridity (AI) values. Given that a later step in the analysis (see the results section) uses downward adjustments to the AI values (Step 5), it was necessary to remove this convergence and new uncertainty bounds were established that were also extended to much lower AI values. The results of this analysis, as well as the equations for the uncertainty bounds, are presented in Appendix 1.

3.2.3. Step 3: constraints compatibility check and establishing behavioural sub-basin parameters

There is no guarantee that the groundwater recharge values of Döll and Fiedler (2008) are compatible with the low flow responses of the observed streamflow. It was therefore necessary to check these as a first step in the application of model version 2. If they are not compatible then the approach will never find any behavioural simulations, regardless of the parameter sets used. Fortunately, the software utilities available (see Ndzabandzaba and Hughes, 2017 for further details and examples) with the model allow these types of incompatibility to be determined quite efficiently. This part of the initial processing therefore established new groundwater recharge constraints where necessary.

The initial model parameter ranges (Table 1A) were established based on previous modelling experience in the Congo River Basin (Tshimanga and Hughes, 2014; Kabuya, 2020). In this study, only model parameters responsible for a sub-basin's natural hydrology (19) are used to simulate behavioural sub-basin responses and five were considered as fixed values, leaving fourteen being considered as uncertain and sampled using a uniform probability distribution.

3.2.4. Step 4: generating total cumulative flows

Model version 3B (Fig. 4) is then run to generate ensembles of total cumulative flow at all of the gauging sites. During this process some of the downstream routing parameters can also be considered fixed or uncertain. No water use parameters were used in this study as all the gauges are considered to represent largely un-developed conditions (Nilsson et al., 2005; Santini and Caporaso, 2018). A further option in versions 3 and 4 (A and B) of the model allows for the parameter sampling across all sub-basins to be totally independent, or grouped according to some (user defined) criteria of sub-basin similarity. In the former, the uncertainty band downstream of a group of sub-basins will be generally lower given that all of the upstream sub-basins will contribute relatively wet or dry incremental simulations in a random manner. In the latter, the sampling scheme is such that generally wetter (or drier) simulations will be linked for all sub-basins in the same group, suggesting a higher band of uncertainty downstream.

3.3. Evaluation of model performance

An additional utility program can be used to post-process the time series ensembles to generate five time series representing the minimum, the 5th, 50th and 95th percentiles and the maximum simulated flows for each month of the total time series. The 5th and 95th percentiles provide useful upper and lower uncertainty bounds covering 90% of all the simulated ensembles and excluding any outliers. It should be noted that the simulation uncertainty bounds are a result of the uncertainty bounds derived from the regional analysis of the hydrological indices that are used to constrain the model in both gauged and ungauged basins (Ndzabandzaba and Hughes, 2017; Kabuya et al., 2020). They are therefore not arbitrary, but represent the uncertainty in our understanding of regional differences in hydrological response. Whether or not the final simulation bounds are appropriate for any specific practical use (e.g. the design of reservoir storage, or abstraction operating rules) is important, but out of the scope of this paper. The simulated uncertainty bounds can be compared with the observed flows at both headwater and downstream gauging stations, using either hydrographs or flow duration curves (FDCs), but other performance measures (Nash and Sutcliffe, 1970; Krause et al., 2005; Moriasi et al., 2007; Wöhling et al., 2013; Waseem et al., 2016) such as Nash-Sutcliffe coefficient of efficiency and mean monthly runoff bias (for both untransformed; NE and%Bias, and transformed values; NE{ln} and%Bias{ln}) can also be used to assess individual ensembles.

In this study, the key performance measures used are based on the extent to which the observed time series, or percentage points on the FDC, fall within the four quartiles representing the uncertainty band of the simulations for the same month or percentage point. Values of 0 and 3 for this containment index represent conditions where the observed data lie at the low or high end of the simulated range, while 1 and 2 indicate that the observed data lie in the middle of the range. Similarly, values of ≤ 1, or ≥ 4 indicate that the observed data fall outside the uncertainty range. The purpose of the results evaluation is therefore to determine how many of the calibration and validation gauges have a high proportion of observed data that fall outside the simulated uncertainty bounds, and to look for any patterns that might point to how the regionalisation can be improved using additional information about the sub-basin characteristics. The key issue is that the observed data are not used directly to calibrate the model, although some of these data are used to develop the hydrological index constraint bounds. The observed data are therefore mainly used to assess the extent to which the constraint bounds can be used to generate appropriate simulations in ungauged sub-basins.

4. Results

4.1. Assessment of the initial groundwater recharge estimates

As mentioned before, it is important to ensure that the ranges of the groundwater recharge estimates (MMR) are compatible with the Q90/MMQ constraint. In many cases, the results have shown that the groundwater recharge values of Döll and Fiedler (2008) were incompatible with the Q90/MMQ constraint and therefore were revised for consistency in the simulation of low flows (Fig. 5) in stage 1 of the modelling framework. Since the original MMR values are model dependant, it was expected that their use in this modelling exercise would constitute one of the major sources of uncertainty associated with low flows. Conversely, there are also some sub-basins in the upper Lualaba, Kasai, Rift valley, and Batéké plateaux where the revised MMR values fall within the original range, suggesting that this global data do have some value for constraining the groundwater components of a hydrological model.

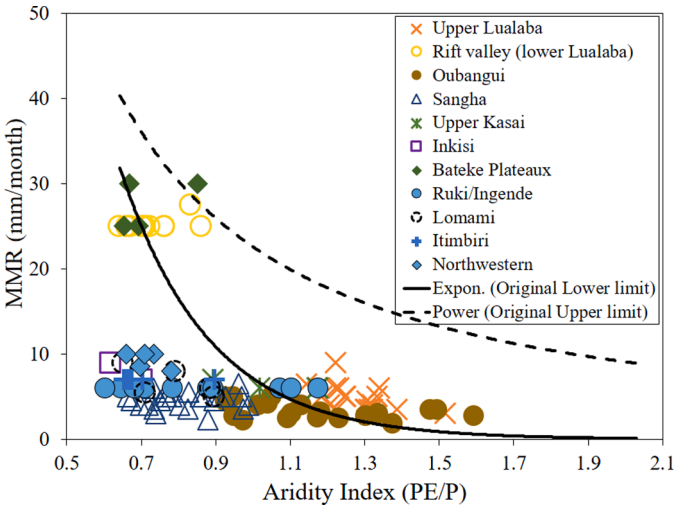

Fig. 5. Revised groundwater estimates after the consistency check with the Q90/MMQ constraint. The dashed and solid lines represent the upper and lower uncertainty bounds of the recharge values of Döll and Fiedler (2008).

4.2. Initial assessment of the results

As noted above, the first step prior to running the model was to check whether adjusments to the constraint values were required given the longer period of modelling compared to the observed data periods used for developing the regionalisation. The large majority of the adjustments required were less than ±5% and most are not considered likely to have any real impact on the results. Table 4 presents the results of the analysis (using the output from the constrained version of the model) based on identifying the number of months in either the time series or the FDCs where the observed data are bracketed by the simulated uncertainty bounds (using the 95% and 5% exceeded values). Columns 3 to 5 list the % number of months in the time series where the observed data are below, within or above the simulated bounds, while columns 6 to 8 repeat this information but using the FDCs. The final three columns list the quartiles of the simulated bounds in which the observed data lie for the three key percentage points. Values between 0 and 3 indicate that the observed data are within the simulated bounds, negative values indicate situations where the observed data are below (i.e. over-simulation), while positive values indicate where the observed data are above (i.e. under-simulation).

The first observation is that even where the FDC results are acceptable (where the last 3 columns of Table 4 are all ≥ 0 or ≤ 3, and a high value for column 7), the% of observed data falling within the simulation bounds for the time series (column 4) is typically quite low (maximum value of ~47% for L_CB261, Fig. 6). This is quite a common issue in data scarce regions where, even if the input gridded climate data are acceptably representative of the overall seasonality and intra-annual variability, individual monthly rainfall values might be poorly representative of reality. This means that the FDCs of the resulting simulated flows may be acceptable, but there may be parts of the time series that are not very well simulated. The second observation is that while there are some sites in both the calibration and validation data sets that show good results (or at least adequate for parts of the FDC, Fig. 7a and 7b), there are also many that are totally inadequate with extremely high positive quartile index values (extreme under-simulation, Fig. 7c), and some quite high negative values (moderate to high over-simulation, Fig. 7d). The remainder of this results section is therefore focused on attempting to resolve some of these discrepancies by identifying possible reasons why the regionalisation has failed in some areas and using the outcomes of this investigation to revise and improve the regioanlisation approach. The order in which the sub-basins are discussed is largely determined by the scale of the discrepancies between the observed data

Table 4
Overall statistics of the simulated flow time series and flow duration curves across gauging stations used in this study, based on both the original (first row of each gauging station code) and revised simulations (from second row of each gauging station code).

SN	Code	Time series			Flow duration curve					
		Below	Within	Above	Below	Within	Above	10%	50%	90%
1	**C_CB138**	5.4	15.0	79.6	4.3	1.1	94.6	6	9	9
	New&New slope	8.6	30.1	61.3	2.2	6.4	91.4	4	5	6
2	C_CB169	4.9	1.9	93.2	3.7	2.4	93.9	9	37	60
	New slope	5.8	13.6	80.5	1.2	16.1	82.7	2	10	30
	Unidel	35.0	11.7	53.2	37.2	16.1	46.7	−4	3	18
	With CL	31.1	21.4	47.5	19.5	39.9	40.6	−2	2	10
3	**C_CB185**	74.2	15.8	10.0	89.2	10.8	0.0	0	−2	−4
	Less rain	47.9	35.3	8.4	24.2	70.0	5.8	3	0	−2
4	C_CB188	17.5	37.5	45.0	5.0	50.8	44.2	2	4	4
	New	20.0	34.2	45.8	4.2	58.3	37.5	2	3	4
5	C_CB218	35.1	23.7	41.2	10.3	49.5	40.2	5	4	0
	New	22.7	34.0	43.3	7.2	34.0	58.8	4	4	−1
6	K_CB259	9.7	19.5	70.8	6.6	8.9	84.5	2	10	10
	With CL	37.7	17.0	45.3	19.5	48.2	32.3	−2	4	5
7	L_CB18	24.8	15.0	60.2	0.3	78.4	21.3	2	2	7
	New	43.6	32.2	24.2	52.2	47.8	0.0	0	−2	1
8	L_CB27	17.1	31.5	51.4	4.2	53.2	42.6	1	3	6
	New	26.9	37.0	36.1	9.7	46.8	43.5	0	3	4
9	L_CB191	1.1	2.3	96.6	0.0	0.0	100.0	22	41	53
	New slope	14.6	25.8	59.5	0.0	0.0	100.0	5	5	12
	New rain	38.2	29.2	32.6	30.3	59.6	10.1	0	−3	2
10	**L_CB196**	13.7	38.2	48.1	6.8	66.7	26.5	1	3	3
	New	35.3	37.3	27.4	16.7	83.3	0.0	−1	1	1
11	L_CB200	8.6	17.1	74.3	8.6	2.8	88.6	4	6	8
	New	8.6	17.1	74.3	5.7	5.7	88.6	6	6	7
12	L_CB201	18.0	29.0	53.0	6.3	93.7	0.0	0	2	3
	New	36.9	43.9	19.2	18.4	81.6	0.0	−1	0	0
13	L_CB202	6.9	23.4	69.7	0.0	16.4	83.6	3	6	6
	New	10.2	22.0	67.8	0.7	12.8	86.5	3	7	5
14	**L_CB203**	28.2	32.0	39.8	5.5	94.5	0.0	2	2	1
	New	32.3	37.8	29.9	11.0	89.0	0.0	3	2	−1
15	**L_CB205**	8.3	46.4	45.3	3.0	61.7	35.3	0	3	4
	New	12.3	54.7	33.0	1.3	98.7	0.0	1	3	3
16	L_CB207	23.3	33.3	43.4	4.9	62.5	32.6	1	2	5
	New	23.6	41.7	34.7	9.7	65.3	25.0	0	2	4
17	L_CB230	3.2	13.6	83.2	1.2	11.1	87.7	3	9	11
	New	3.7	17.0	79.3	1.7	12.1	86.2	3	8	10
18	**L_CB261**	29.8	47.3	22.9	12.1	87.8	0.0	0	1	0
	New	32.1	44.3	23.6	19.8	80.2	0.0	0	1	−1
19	O_CB76	38.4	40.6	21.0	8.1	91.9	0.0	0	0	1
	New	40.6	49.4	10.0	10.7	89.3	0.0	0	1	0
20	**O_CB95**	25.8	45.4	28.8	7.7	83.8	8.5	0	1	3
	New	33.9	47.6	18.5	7.7	92.3	0.0	0	0	2
21	**O_CB176**	25.1	25.5	49.4	9.2	53.1	37.7	4	3	1
	New	28.2	28.2	43.6	13.8	52.3	33.9	2	3	0
22	**O_CB179**	41.6	42.8	16.4	42.5	57.5	0.0	2	0	−2
	New	44.4	37.7	17.9	34.9	65.1	0.0	2	0	−1
23	**O_CB181**	37.3	32.5	30.2	30.6	67.5	1.9	2	0	1
	New	46.4	32.8	20.8	57.4	42.6	0.0	2	0	−1
24	**O_CB355**	16.2	42.8	41.0	3.1	66.7	30.2	1	2	3
	New	17.1	35.6	47.3	7.7	27.0	65.3	1	4	2
25	S_CB55	57.7	27.0	15.3	62.7	37.3	0.0	0	0	−4
	New	48.7	33.7	17.6	31.3	68.7	0.0	−1	1	−1
26	S_CB61	31.3	25.3	43.4	8.1	87.8	4.1	2	2	2
	New	25.9	40.6	33.5	5.6	94.4	0.0	1	2	2
27	**S_CB134**	72.0	22.7	5.3	94.0	6.0	0.0	−1	−2	−5
	New	28.0	31.3	10.7	63.3	36.7	0.0	−2	−1	−3
28	**S_CB158**	30.5	37.4	32.1	10.6	88.4	1.0	−1	2	2
	New	29.1	42.7	28.2	10.3	88.4	1.3	0	2	2
29	**S_CB236**	58.5	22.0	19.5	53.5	46.5	0.0	−1	1	−5
	New	48.0	28.0	24.0	31.5	68.5	0.0	0	1	−1
30	**S_CB243**	24.2	21.4	54.3	12.6	45.6	41.8	−1	3	5
	New	25.8	36.8	37.3	12.1	66.5	21.4	−1	2	4
31	**S_CB395**	23.3	27.3	49.4	5.2	68.8	26.0	2	3	3
	New	23.7	35.3	41.0	4.6	61.9	33.5	3	4	2

Footnote: Purple colour indicates acceptable results based on FDC and blue good results (or at least adequate for parts of the FDC) based on the original constraints developed by Kabuya et al. (2020). The sub-basin code in bold refers to the calibration gauging stations as already shown in Table 1. The first row of each gauging station shows the results using the original and subsequent other rows show revised simulations after applying: **(i)** slope adjustment factor (New slope), **(ii)** adjusted rainfall estimates (New rain), **(iii)** Unidel rainfall data (Unidel), **(iv)** channel routing parameter (With CL), **(v)** scaled rainfall (Less rain) and re-run of the model after the convergence of the uncertainty bounds at low AI values was removed (New). "New" refers to revised results based on adjustments to the input parameter bounds to try and achieve a more even distribution of the outputs relative to the input constraint bounds (see text for more detail).

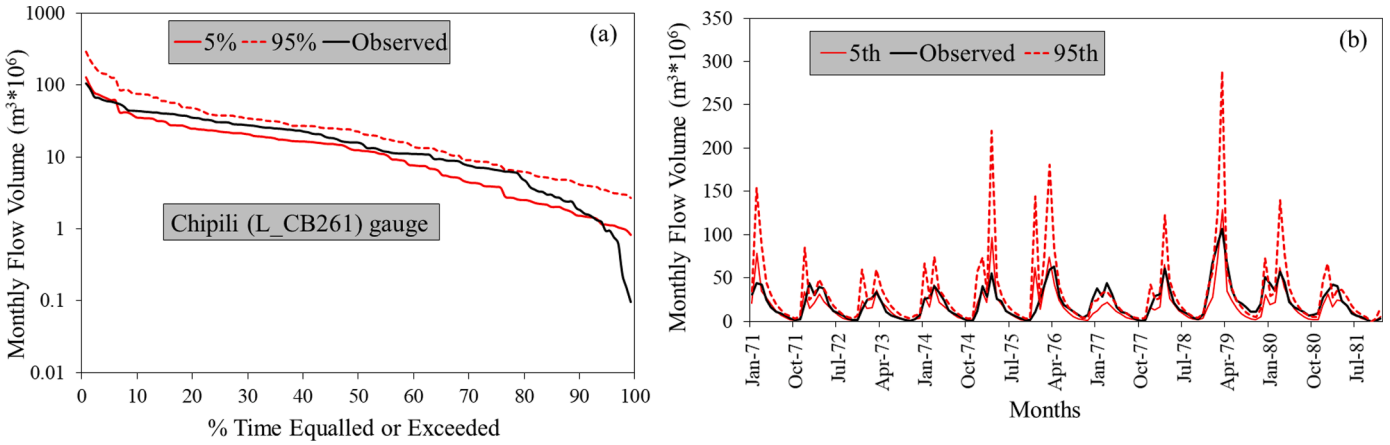

Fig. 6. Simulated uncertainty bounds of the flow duration curve (a) and the time series (b) at the Chipili (L_CB261) gauging station in the upper Lualaba.

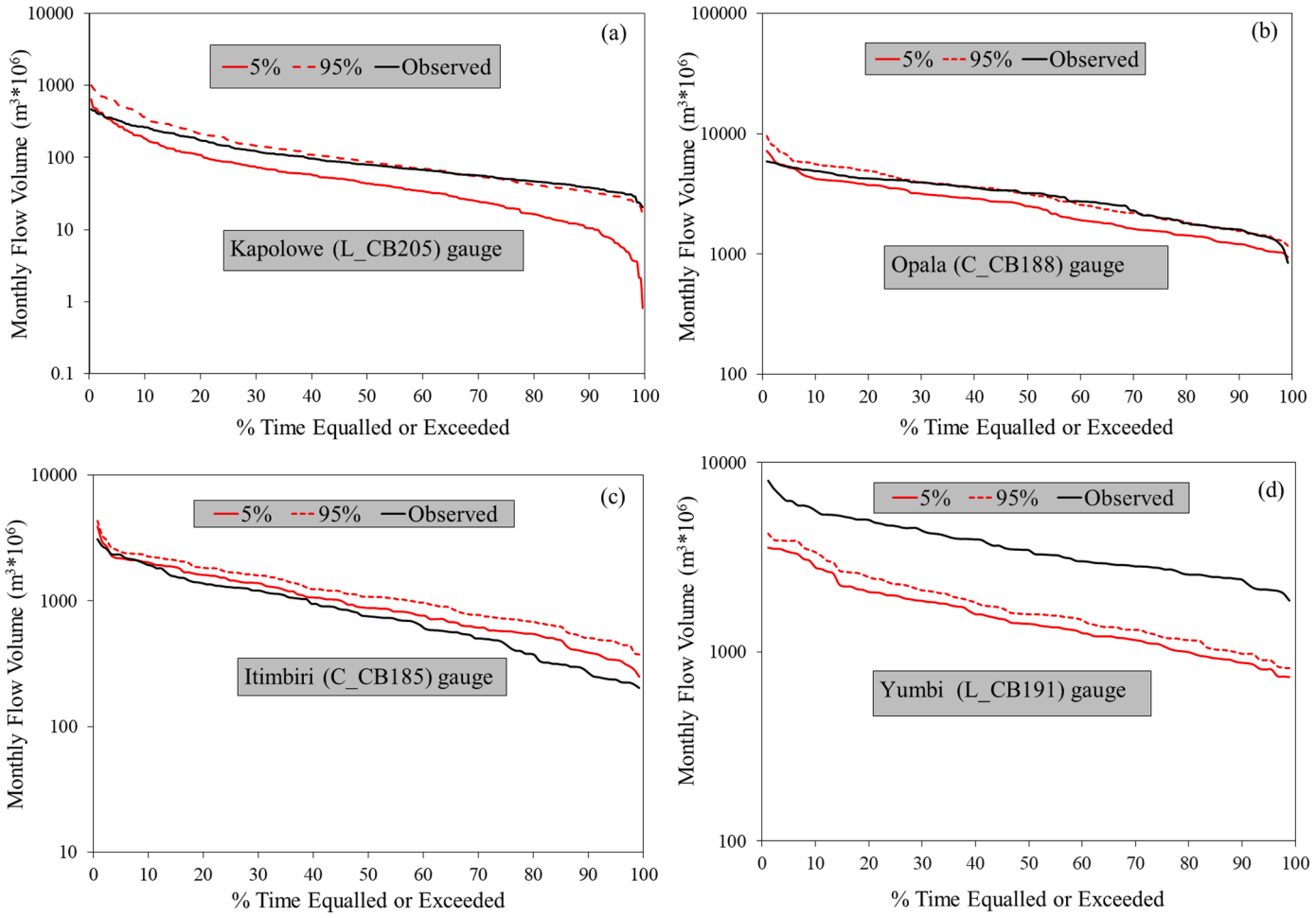

Fig. 7. Simulated uncertainty bounds showing different situations of acceptable upper FDC (a), acceptable parts of FDC (b), moderate over-simulation (c) and extreme under-simulation (d).

and the simulated uncertainty bounds.

4.3. Reassessment of the results

One of the largest discrepancies between the simulations and the observed data occur for L_CB191 (a total of 12 sub-basins lying near the rift valley to the west of Rwanda) and it is immediately evident that this area has high slopes (>10%, and some >20%) relative to nearly all the rest of the Congo River Basin. This observation prompted the use of a slope correction factor to reduce the aridity index in sub-basins with slopes greater than about 7%. After some trial and error attempts to find a suitable correction approach, Eqs. (1) and (2) were used for adjusting the aridity index (AI) that is applied to the regional estimation equations for MMQ and Q90/MMQ, with the condition that the adjustment factors are limited to a maximum value of 1. For slopes of 8% or less, both adjustment factors are relatively close to 1, while for a slope of 20%, the

MMQ adjustment factor is 0.3 and the Q90 factor is 0.7. Reference to Fig. 2 suggests that the effects of reducing the AI value by these amounts will vary with the original AI value and have a large effect for AI values of less than about 0.8. The rationale for a lower Q90 correction factor is that the actual Q90 value will be affected by both an increase in the MMQ constraints, as well as in the Q90/MMQ constraint. The adjustment factor required for the AI value used with the Q10/MMQ and Q50/MMQ relationships was expected to be less and was set to half way between 1 and the $AI_{Adj}Q90$ value. The format of Eqs. (1) and (2) was largely guided by the initial results for L_CB191, but C_CB138 and C_CB169 also included sub-basins with quite high slopes and can therefore be used to test the slope adjustments.

$$AI_{Adj}MMQ = (\ln(slope))^{-3} \times 8 \quad (1)$$

$$AI_{Adj}Q90 = (\ln(slope))^{-1} \times 2.1 \quad (2)$$

After applying the slope adjustments to L_CB191 the results improved substantially (Table 4, 2nd row for L_CB191), but the under-simulation remained. It was further noted that many of the sub-basins in the upper parts of the catchment have lower CRU rainfall (and higher AI values) than the lower areas, which appears to be somewhat counter-intuitive. The UNIDEL rainfall data also show a similar pattern, but the rainfall based on a water balance (Table 5) using MODIS actual evapotranspiration data (Observed runoff depth + MODIS AET) suggest rainfalls that are much higher for the upper parts of the catchment. After the lower rainfall sub-basins were adjusted to increase the total basin weighted rainfall by some 15%, the results improved substantially (Table 4, 3rd row for L_CB191). The rainfall adjustments applied were very simplified, given the lack of any detailed evidence that could be used for individual sub-basins. It is also acknowledged that the evidence for the adjustments is not very precise, given the uncertainties inherent in the MODIS AET estimates. However, the balance of evidence suggests that they are justified, even if the actual adjustments are not likely to be at all accurate.

For C_CB169 (Batéké plateaux) the original results suggest very high levels of under-simulation for moderate to low flows and the observed flow duration curve has a very low slope which is inconsistent with the simulated constraint ranges. The slopes are generally quite high (9.5 to 13.3) and the slope adjustments certainly improve the simulations (Table 4). The UNIDEL rainfall is some 14% higher than the CRU data (Table 5), and if the UNIDEL data are used to force the model, not only will there be more rainfall available but the AI values also decrease, both of which improve the simulations (Table 4, 3rd row for C_CB169), but low flows remain under-simulated. These sub-basins are the main ones draining the Batéké Plateaux and the major river valleys are deeply incised with floodplain wetlands. This suggests the possibility of some high flow attenuation, which was roughly simulated using uncertain ranges for the channel routing parameter in the second stage run of the model (i.e. not affecting the sub-basin incremental flow simulations driven by the estimated constraint ranges, but only the routing through the sub-basins). This improves the results further (Table 4, 4rd row for C_CB169), despite the approach being a very simplified way of accounting for possible floodplain and wetland attenuation effects.

The original results for C_CB138 (Inkisi) suggest quite high levels of under-simulation, notably for low flows and the influence of the slope adjustments is quite small as the slopes are mostly about 8% or less. There is some evidence from the water balance calculations (Table 5) that the rainfall might be slightly under-estimated and there is some evidence that the MMQ value based on the relatively short observed data period (1951 to 1959) under-represents the long-term MMQ by some 10%. Applying these adjustments gives slightly better results (Table 4), but the observed flows remain under-simulated.

The observed flows for K_CB259 (upper Kasai) are quite highly under-simulated for moderate to low flows (Table 4). The slopes are all quite low, but the basin is long and quite narrow, suggesting that channel attenuation may play a role. Applying the channel routing parameter gives some improvements and this could have implications for other ungauged rivers in the south western partf of the Congo River Basin, many of which have similar basin shape characteristics (Fig. 1). L_CB200, 201 and 202 are gauged sub-basins of LCB18 (Table 2), while L_CB230 is in the same area. While the results for the downstream site (L_CB18, Table 4) improved, the results for the smaller headwater catchments did not change much with some being under- and others being over-simulated. L_CB200, LCB202 and L_CB230 remain quite highly under-simulated for moderate to low flows and there is no currently available evidence to suggest why this region has an apparently different low flow regime than other parts of the total basin. However, previous work (unpublished, but including field observations) in these Zambian catchments confirm that sustained flows occur throughout the dry season. It is possible that there is an influence related to geology, but we were unable to identify any data sources that could suggest any unique characteristics of the geology that would contribute to sustaining low flows.

C_CB185 (Itimbiri) is generally over-simulated, particularly for moderate to low flows, while the slope adjustment changes do not affect this set of sub-basins. The water balance check using MODIS AET data (Table 5) suggest that both the CRU and UNIDEL rainfalls could tend to over-estimate the available moisture and the constraints were re-set and the model re-run with the CRU rainfall data scaled by 94%. The results are certainly better, with low flows still being somewhat over-simulated (Table 4). The results for the remaining sub-basins were generally quite good, or only moderate over- or under-simulated and the revisions did not change the situation very much with some improving slightly and others being somewhat poorer. However, Table 4 indicates that in general terms the revisions have generated improved results. S_CB236 (in the northwestern sub-basins) represents one of the few sub-basins where there is a relatively large difference between the MMQ for the short observation period (1951 to 1970) and the longer simulation period. However, the overall result did not change very much. It is also an area that has very high forest cover and one of the changes that was made was based on turning off the surface runoff generation part of the model and simulating all flows as either interflow or groundwater discharge. This improved the results (Table 4) partly because the final simulations had a larger uncertainty range than the original ones based partly on surface runoff generation.

Table 5
Examples of the water balance analysis.

SN	Code	Water Balance components				
		Stream flows (mm y^{-1})	MODIS AET (mm y^{-1})	Rainfall water balance (mm y^{-1})	CRU rainfall (mm y^{-1})	UNIDEL rainfall (mm y^{-1})
1	**C_CB138**	419.1	814.8	1234.0	1388.9	1363.9
2	C_CB169	809.9	732.8	1542.7	1685.0	1916.1
3	**C_CB185**	320.6	1106.3	1426.9	1698.5	1643.2
4	C_CB218	839.5	989.0	1828.6	1849.5	1988.0
5	L_CB191	1060.7	929.2	1990.0	1389.1	1678.4
6	O_CB76	262.7	640.7	903.3	1547.1	1534.3
7	**O_CB95**	133.2	384.6	517.7	1324.0	NA
8	**O_CB176**	347.6	609.7	957.3	1485.7	1480.0
9	**O_CB179**	209.5	528.3	737.8	1459.0	1380.3

5. Discussion

Fig. 8 illustrates the frequency distributions of the containment indices for the original and revised simulations. It is evident that there are relatively few changes in the Q10 and Q50 indices, apart from the fact that some of the small number of large under-simulations have been improved. There are also quite a high number (≥20) gauging stations where the observed data were totally within both the original and revised simulated bounds. There are far fewer (<15) gauging stations

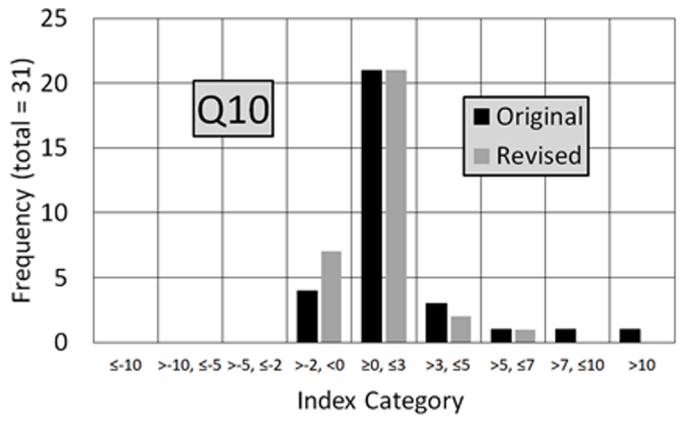

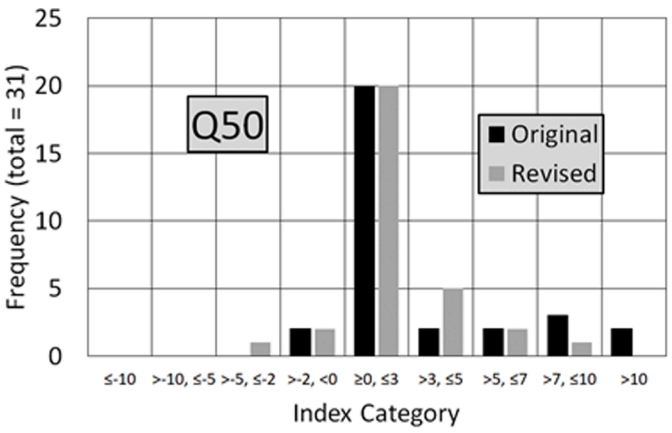

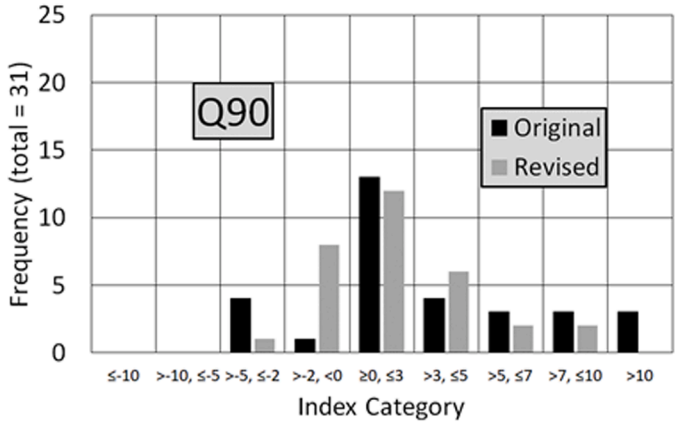

Index Category	Explanation
≤-10	Large over-simulation
>-10, ≤-5	Moderate to large over-simulation
>-5, ≤-2	Minor to moderate over-simulation
>-2, <0	Minor over-simulation
≥0, ≤3	Observed within simulation bounds
>3, ≤5	Minor under-simulation
>5, ≤7	Minor to moderate under-simulation
>7, ≤10	Moderate to large under-simulation
>10	Large under-simulation

Fig. 8. Frequency distributions of the indices used to determine the containment of observed flows within the simulated flow duration curve bounds.

where the low flows (Q90) are successfully simulated, and there remain quite a high number where the low flows are either under-simulated (mostly), or over-simulated after the revisions to the constraint values. This result could almost have been predicted, given the large spread in Q90/MMQ values shown in Fig. A1 (Appendix 1). While some of the identified adjustments have improved the situation, there are evidently other factors that have not been accounted for that cause quite large differences in low flow response in different parts of the Congo River Basin. Some of the adjustments made have been based on including the channel routing parameter to attenuate high flows and increase lower flows. This parameter has the greatest impact on downstream flows from a number of upstream sub-basins and has already been justified in some sub-basins (C_CB169 and K_CB259), but it may also apply in others where there is expected to be high flow attenuation. However, it is not a simple matter to identify those areas where the use of the channel routing parameter can be justified based on measurable physical characteristics (Tshimanga and Hughes, 2014).

Differences in land cover have not been taken into account in the regional analysis of the constraint values, largely because there were no clear signals in the orginal analysis (Kabuya et al., 2020b), possibly because of the relatively small data set. There are also no clear signals in the current analysis and therefore the effects of land cover on runoff ratio and the shapes of FDCs remain largely unknown for the Congo River Basin. The effects of increased evapotranspiration losses from forestry areas has largely been accounted for through uncertainty ranges in the annual potential evaporation demand, but differences in this range have not been fully related to the area of forest cover. The lower value of the range has been set to the IWMI estimates (http://www.iwmi.org), which could under-estimate evapotranspiration losses in densely forested areas. However, this would mainly increase the simulated range of at least some of the constraint indices.

During the simulation runs it was noted that some of the simulated ranges were relatively low, and certainly lower than the input constraint ranges. This has the potential to exacerbate any over- or under-estimates relative to observed data as the quartiles of the simulated range will be quite small. It is therefore considered to be important to ensure that the simulated ensembles cover the range of the input constraints (i.e. are not biased to either extreme, or concentrated in a small part of the range), to ensure that the results reflect the input constraints rather than any bias in the model simulations within these constraints. However, this is not always straightforward to achieve, given the large parameter space and inherent equifinalities (Hughes, 2016; Her and Seong, 2018). One observation is that it is often better to fix some of the parameters to achieve more clearer control over the uncertainty in the outputs (i.e. reduce the equifinality in the uncertainty). The situation for S_CB236 (including S_CB332) illustrates this problem, in that the original simulated range of the Q10/MMQ constraint was always limited to a narrow band within the middle of the input range. Various combinations of the surface runoff parameters affecting high flows made very little difference to this result, while turning off the surface runoff generation parameters and focusing on simulating high flows with the interflow function made a large difference. This is a justifiable result for a heavily forested area and it would be worthwhile to assess whether this approach would be beneficial in other heavily forested areas, despite the fact that many of these already have acceptable results. It should be noted that in the case of S_CB236 (Table 4), all of the observed values for the constraint indices are well within the regionalised uncertainty ranges input to the model. It is therefore evident that at least some of the results that show containment indices that are just outside of the ideal range of 0 to 3 are a modelling artefact where the observed data are

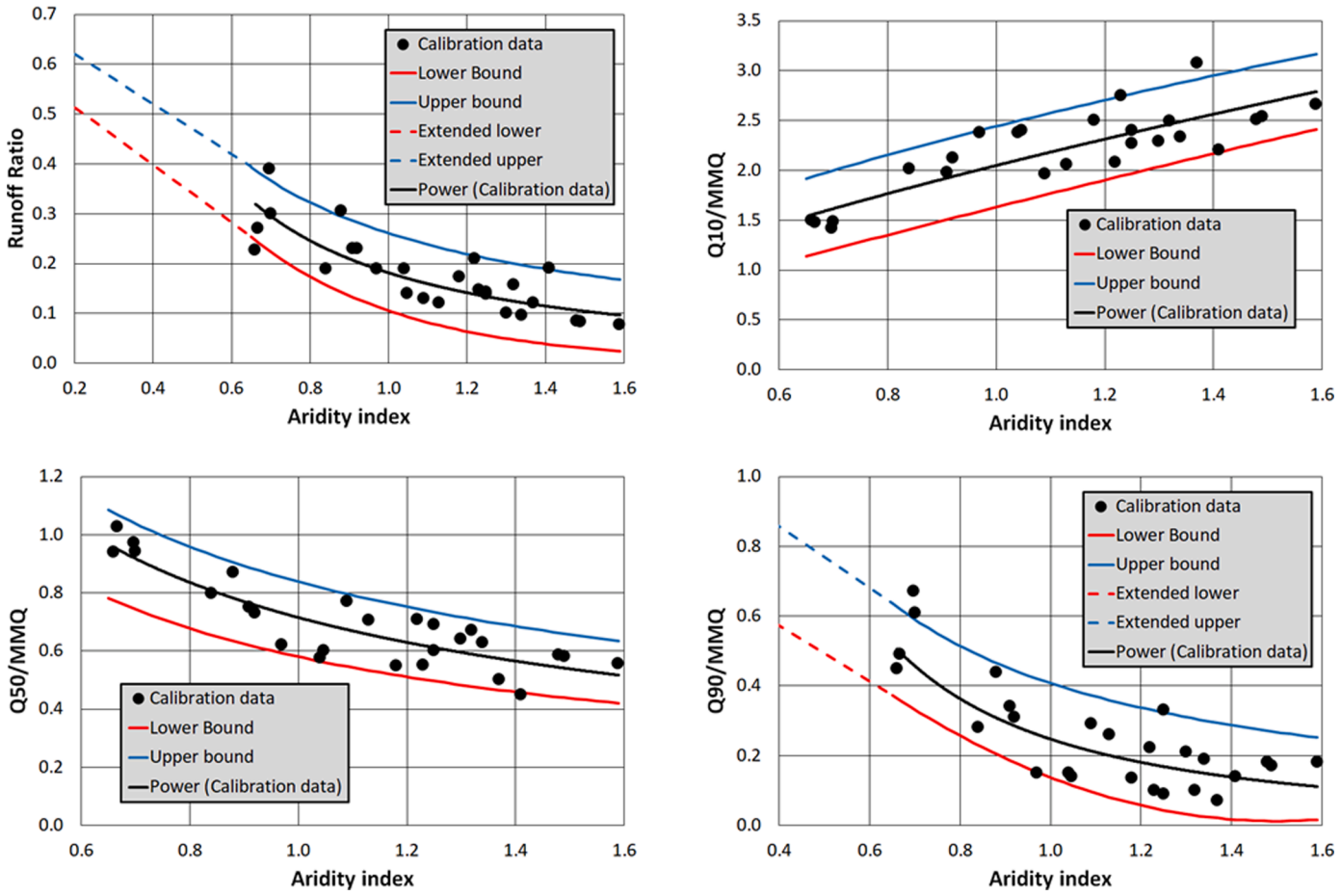

Fig. A1. Regression relationships and uncertainty bounds for the four main constraints (the ardity index is extended downwards for the Runoff ratio and Q90/MMQ constraints to account for lower values due to the higher adjustments based on slope).

inside the input constraint ranges, but the model has generated an output range that is narrower and biased toward one end of the input range.

The same principles could be applied to C_CB218 (Ruki/Ingende) which has 10 sub-basins (Table 2), all of which are forested. One of the observations is that, while the observed data have values for the constraint indices that fall within the input uncertainty range, the observed Q50/MMQ and Q90/MMQ are close to the upper end of the uncertainty range. The UNIDEL rainfall data are some 8% higher than the CRU data and using the UNIDEL data has the effect of lowering the aridity index which in turn, increases the runoff ratio, Q50/MMQ and Q90/MMQ, while slightly decreasing the Q10/MMQ constraint. This effect places the observed constraint indices more within the input constrain ranges, as well as providing more water. *Re*-running the model with the new constraints and the increased rainfall improved the results with the three key containment indices largely improving (Q10=3, Q50=1, and Q90=−2). The Nash-Sutcliffe efficiency values also improved from approximately 0.3 (for both untransformed and ln transformed data) to values of better than 0.55 across the ensemble set. This result offers further support for replacing the CRU rainfall data with the UNIDEL data for this set of sub-basins. It was also noted that the short record (97 months of available data) creates an observed FDC that is not smooth and with quite large changes within a few percentage points, particularly at the extremes, making the containment results very sensitive to the exact percentage points chosen for comparison. The overall result shows the ensemble of flow duration curves that were very close to the observed data for the most part, but this was achieved with a low uncertainty range, which meant that even relatively small deviations outside this range by the observed values lead to poor containment index values at some percentage points. The conclusion for this site is that possible problems with the rainfall data (possibly also the short record of observed flows) combined with possible effects of forestry make the original constraint indices inappropriate.Table 1A.

One of the issues that is extremely difficult to account for is uncertainties in the observed streamflow, input rainfall and evaporation demand data, largely because there are not enough alternative datasets to confirm or deny the appropriateness of the data that have been used. Some attempts were made to use MODIS AET data and alternative rainfall data sets (UNIDEL) to assess the validity of the CRU data. In some cases this analysis pointed to some potential problems in the CRU data, but the MODIS data are also very uncertain (Ruhoff et al., 2013; Velpuri et al., 2013), as evidenced by some very low values in some areas (Table 5). The effects of all these data uncertainties has a compound effect. They not only affect the simulations themselves (e.g. not enough rainfall to force the model to achieve the observed outputs, as noted for parts of L_CB191), but they also affect the regional relationships that are used to quantify the input constraint values, because they impact on the aridity estimates (Kabuya et al., 2020b). Given that these compound effects could be quite different for each of the sub-areas used in this analysis (i.e. the uncertainties are likely to be quite random in their effects), it is very difficult to resolve them to improve the results.

It is important to note that the model can be calibrated to closely reproduce the shapes of all the observed flow duration curves, even if the statistics of fit for the time series can frequently be quite poor (e.g. Nash Sutcliffe efficieny values of less then 0.4 in Kabuya, 2020). The key issue is therefore not that the model cannot be parameterised to generate appropriate responses, but that the constraints (which are model independent), in combination with the input forcing data used, do not

Table 1A
Initial model parameter range values used across different drainage systems of the Congo Basin.

Drainage system		RDF	PI1	SER	ZMIN	ZAV	ZMAX	ST	POW	FT	GW	R	TL	CL	GPOW	DDENS	T	S	RGWS	GWL	RSF
Kasai	Mean	0.6	2	1	69.4	0.3	728.4	1200	3.6	30	20.4	0.4	0.3	0	3.3	0.5	32	0.1	0	15	1
	Dist. type		3	3	3	3	3	3	3	3	3.0	3			3		3				3
	Min	0.6	2	0.7	45	0.3	650	900	3	30	10.0	0.3	0.2	0	3	0.2	30	0	0	10	1
	Max	0.8	4	1	70	0.5	900	1250	4	50	30.0	0.6	0.3	0	4	0.5	50	0.1	0	30	2.5
Lomami	Mean	0.6	1.5	1.0	75.0	0.2	900.0	1800.0	4.0	15.0	15.0	0.6	0.3	0.0	3.5	0.4	40.0	0.0	0.0	15.0	1.8
	Dist. type		3.0	3.0	3.0	3.0	3.0	3.0	3.0	3.0	3.0	3.0			3.0						3.0
	Min	0.6	2.0	0.3	50.0	0.2	800.0	1400.0	3.0	10.0	5.0	0.3	0.2	0.0	3.0	0.2	20.0	0.0	0.0	10.0	0.6
	Max	1.2	4.0	1.0	120.0	0.4	1100.0	1800.0	4.0	35.0	20.0	0.7	0.8	0.6	4.0	0.7	50.0	0.0	0.0	50.0	2.0
Lower Congo	Mean	1.2	2	1	31	0.6	590	680	3.9	40	60.0	0.4	0.3	0	5	0.5	30	0.1	0	25	1.1
	Dist. type		3	3	3	3	3	3	3	3	3.0	3			3		3				3
	Min	0.6	1.2	0.3	15	0.2	1000	650	3	60	50.0	0.2	0	0	3	0	30	0	0	0	0.5
	Max	1.2	3	1	60	0.6	1300	1050	4.5	90	70.0	0.6	0	0	4.5	0	70	0.1	0.1	0	2
Lualaba	Mean	0.7	2.1	0.9	144	0.4	677.5	730.7	4.2	29.3	23.8	0.3	0.3	0	3.8	0.5	25	0	0	15	1.4
	Dist. type		3	3	3	3	3	3	3	3	3.0	3			3		3				3
	Min	0.6	2	0.9	140	0.3	600	500	3.5	20.0	15.0	0	0.2	0	3.5	0.2	8	0	0	5	0.5
	Max	0.8	4	1	180	0.5	900	800	4.5	37.0	30.0	0.5	0.3	1	4.5	0.5	30	0.1	0	15	1.5
Oubangui	Mean	0.6	1.5	1.0	50.0	0.2	900.0	1800.0	4.0	15.0	15.0	0.6	0.3	0.0	3.5	0.4	40.0	0.0	0.0	25.0	1.5
	Dist. type		3.0	3.0	3.0	3.0	3.0	3.0	3.0	3.0	3.0	3.0			3.0		3.0				
	Min	0.6	1.5	0.4	40.0	0.1	400.0	950.0	2.5	12.0	5.0	0.0	0.2	0.0	3.0	0.2	50.0	0.0	0.0	10.0	0.6
	Max	1.2	3.0	1.0	100.0	0.5	800.0	1400.0	4.5	35.0	12.0	0.5	0.3	0.0	4.0	0.7	70.0	0.0	0.0	50.0	2.0
Ruki	Mean	0.6	1.8	1.0	90.0	0.3	650.0	1800.0	3.8	28.0	10.0	0.3	0.3	0.0	3.5	0.4	57.0	0.0	0.0	25.0	1.5
	Dist. type		3.0	3.0	3.0	3.0	3.0	3.0	3.0	3.0	3.0	3.0			3.0		3.0				
	Min	0.6	1.2	0.7	60.0	0.2	500.0	1600.0	3.5	15.0	5.0	0.2	0.2	0.0	3.0	0.2	40.0	0.0	0.0	10.0	0.6
	Max	1.2	3.0	1.0	120.0	0.5	800.0	1850.0	4.5	40.0	15.0	0.5	0.3	0.0	4.0	0.7	74.0	0.0	0.0	50.0	2.0
Sangha	Mean	0.6	1.8	1.0	90.0	0.3	650.0	1800.0	3.8	28.0	10.0	0.3	0.3	0.0	3.5	0.4	57.0	0.0	0.0	25.0	1.5
	Dist. type		3.0	3.0	3.0	3.0	3.0	3.0	3.0	3.0	3.0	3.0			3.0		3.0				
	Min	0.6	1.2	0.7	60.0	0.2	500.0	1600.0	3.5	15.0	5.0	0.2	0.2	0.0	3.0	0.2	40.0	0.0	0.0	10.0	0.6
	Max	1.2	3.0	1.0	120.0	0.5	800.0	1850.0	4.5	40.0	15.0	0.5	0.3	0.0	4.0	0.7	74.0	0.0	0.0	50.0	2.0

generate outputs that are always a match to the observed data. There are some situations where the model is not able to generate ensembles with constraint index values that are evenly distributed across the various input constraint ranges. This is possibly because some parts of the input constraint ranges are incompatible with each other and the model is not able to generate ensembles that match the full ranges of multiple constraints. One of the consequences of this is that the final uncertainty range of ensembles is much narrower than the input range of the constraints and even if the observed data are close (but not within the range), the containment indices suggest a poor fit. Notwithstanding these rather negative comments about the results, Fig. 8 suggests that quite for a large proportion of the sub-basins the results are quite good, while the details for all sub-basins in Table 4 suggests that there is no real difference between the calibration and validation sites.

6. Conclusions

The overall conclusion is that the orginal regionalised constraint indices based soley on aridity index are appropriate in many sub-basins, but not all. Further detailed examination of these results suggested that the effects of high slopes (prevelant in a relatively small number of sub-basins) could increase the runoff ratio and Q90/MMQ values and that implementing an adjustment factor based on slope did improve some of the very poor results. However, it was also clear that some of the CRU rainfall data under-represented the real rainfall in some areas and this also removed some of the gross under-simulations. It was recognised that there are missing data in the CRU dataset at the start and ends of the total record (these are represented by mean monthly values in the time series), an indication that there are few local data available to generate the gridded values. The worst affected areas (the most years with mean monthly values) stretches across the total basin in a band from the south west to the north east, and mainly covers sub-basins C_CB188 and C_CB218 used in this analysis, but also covers many ungauged sub-basins not included here. Attempts to apply a water balance approach using observed flows plus MODIS AET data to compare with the available rainfall data, were largely inconclusive because of some clearly incorrect MODIS values. Future studies ideally need to more critically assess the rainfall data used to force the model, and in the absence of data to validate any rainfall products, could consider the use of uncertain rainfall inputs into the model using a range of different rainfall products (including satellite derived estimates) to quantify the uncertainties. Multiple information sources of remote sensing products (e.g. satellite water level observations; Jung et al., 2010) may be also useful in the larger rivers to supplement in situ observations.

Some minor improvements were made through the use of the channel routing parameter to reduce high flows and this approach was applied where there is some evidence that upstream high flows could be attenuated. However, this concept was not applied to all other sub-basins, partly because it is not always straightforward to identify where attenuation effects might be applicable. There is some evidence that land cover, and particularly the effects of dense tropical forest should be part of the approach to the regional estimation of the constraint indices. However, once again, this result is far from conclusive as the effects do not appear to apply to all the sub-basins that have high proportions of forest. One of the recommendations for further work is that this issue should be investigated in more detail, both from an empirical (i.e. looking at response differences across all forested areas using the available observed data), and conceptual persepective. The conceptual perspective should include considerations of the likely runoff generation processes across all forested areas and how these should be represented in the model parameter sets.

Some of the sub-basins in the Zambian part of the Congo River Basin appear to have very sustained dry season low flows, resulting in higher Q90/MMQ values than other areas and certainly values that are at the very high end of the regional ranges for this constraint index. We could not find any information that would explain this characteristic of the flow regimes, and this also requires further investigation.

There is some evidence to suggest that sites with quite short records (less than 10 years) and sites with high proportions of missing data can skew the results, even though only the simulated values that were matched with available observed data were included in the containment analysis. There is very little that can be done to improve this situation, although it is possible that some form of observed flow data patching could be attempted. This type of approach, however, might simply end up adding another layer of uncertainty into an analysis that is already very uncertain.

It should be noted that previous work (Tshimanga et al., 2011; Tshimanga and Hughes, 2014) conducted in the Congo Basin has demonstrated that the Pitman model can be calibrated with acceptable statistics in most gauged basins (Nash-Sutcliffe coefficient of efficiency for the majority of the gauging stations range from 0.5 to 0.9) and is therefore considered applicable to the region. However, this does not help to decide how to set the model up for all the many ungauged sub-basins in the remainder of the basin. The current paper attempted to address this problem by applying regionalised indices of sub-basin hydrological response characteristics, and testing the approach using the same gauged basins used in the regionalisation, as well as a set of validation gauging stations that were not previously used. Most of the validation stations are downstream of multiple sub-basins and therefore the validations are based on applying the regional constraint indices to sub-basins and then assess whether the cumulative simulated flow bounds at the gauges are comparable to the observed data in terms of both FDC characteristics as well as their time series variations. This study has not reported on the differences between parameter values across the sub-basins, partly because this would take up a great deal of space in an already lengthy paper, and partly because the main focus of the study was to evaluate the regionalised constraint indices, which are model independent. However, it is recommended that future studies should look at this issue more closely and try to ensure that there is a degree of consistency in the way in which the responses of sub-basins with similar characteristics are simulated by the model.

CRediT authorship contribution statement

Pierre M. Kabuya: Conceptualization, Methodology, Writing – original draft, Writing – review & editing. **Denis A. Hughes:** Supervision, Software, Writing – review & editing. **Raphael M. Tshimanga:** Data curation. **Mark A. Trigg:** Writing – review & editing. **Paul Bates:** Writing – review & editing.

Declaration of Competing Interest

The authors declare that they have no known competing financial interests or personal relationships that could have appeared to influence the work reported in this paper.

Acknowledgements

The authors acknowledge the funding support of the Congo River user Hydraulics and Morphology (CRuHM) project, which is wholly funded by The Royal Society-DFID Africa Capacity Building (RS-DFID) under the grant number “AQ150005”. Paul Bates is supported by a Royal Society Wolfson research Merit award. The modelling tools (Spatsim and Pitman model) used in this study have been developed at the Institute for Water Research/Rhodes University and can be accessed through the Rhodes University website: https://www.ru.ac.za/iwr/research/software/spatsim/. The model setup for the Congo can be accessed by directly contacting the corresponding author.

Appendix 1. Re-assessment of the constraint index regional relationship uncertainty bounds

The Runoff Ratio (RR: used to calculate MMQ) bounds required extending to account for lower aridity index (AI) values after they have been adjusted downwards by the effect of slope. The extensions of the two bounds are based on linear extrapolation of the slopes of the main bound relationships fitted to the 5% and 95% confidence limits of the regression equations (Eqs. (A1) and (A2)) between AI values of 0.75 and 0.65. Fig. A1(a) suggests that this approach may under-estimate the upper bound values for low AI:

For AI values ≥ 0.65

$$RR_{Lower} = 1.2944 \times \exp^{-2.508 \times AI} \quad (A1)$$

$$RR_{Upper} = 0.2608 \times AI^{-0.951} \quad (A2)$$

For AI values < 0.65

$$RR_{Lower} = 0.254 + 0.5758 \times (0.65 - AI) \quad (A3)$$

$$RR_{Upper} = 0.395 + 0.5 \times (0.65 - AI) \quad (A4)$$

The Q90/MMQ bounds also needed extending and the same approach was used:

For AI values ≥ 0.65

$$Q90/MMQ_{Lower} = 0.4975 \times AI^2 - 1.4935 \times AI + 1.1334 \quad (A5)$$

$$Q90/MMQ_{Upper} = 0.4077 \times AI^{-1.037} \quad (A6)$$

For AI values < 0.65

$$Q90/MMQ_{Lower} = 0.373 + 0.8 \times (0.65 - AI) \quad (A7)$$

$$Q90/MMQ_{Upper} = 0.637 + 0.879 \times (0.65 - AI) \quad (A8)$$

There is no need to extend the Q10/MMQ and Q50/MMQ bound relationships as the slope adjustments are smaller and the relationships fitted to the confidence limits are smoother without any signs of convergence at low or high AI values:

$$Q10/MMQ_{Lower} = 1.635 \times AI^{0.843} \quad (A10)$$

$$Q10/MMQ_{Upper} = 2.4425 \times AI^{0.5614} \quad (A11)$$

$$Q50/MMQ_{Lower} = 0.58 \times AI^{-0.695} \quad (A12)$$

$$Q50/MMQ_{Upper} = 0.8383 \times AI^{-0.599} \quad (A13)$$

References

Almeida, S., Le Vine, N., McIntyre, N., Wagener, T., Buytaert, W., 2016. Accounting for dependencies in regionalized signatures for predictions in ungauged catchments. Hydrol. Earth Syst. Sci. 20 (2), 887–901. https://doi.org/10.5194/hess-20-887-2016.

Aloysius, N., Saiers, J., 2017. Simulated hydrologic response to projected changes in precipitation and temperature in the Congo River Basin. Hydrol. Earth Syst. Sci. 21 (8), 4115–4130. https://doi.org/10.5194/hess-21-4115-2017.

Alsdorf, D., Beighley, E., Laraque, A., Lee, H., Tshimanga, R., O'Loughlin, F., Mahé, G., Dinga, B., Moukandi, G., Spencer, R.G.M., 2016. Opportunities for hydrologic research in the Congo River Basin. Rev. Geophys. 54, 378–409. https://doi.org/10.1002/2016RG000517.

Beck, H., De Roo, A., Van Dijk, A.I.J.M., 2015. Global maps of streamflow characteristics based on observations from several thousand catchments. J. Hydrometeorol. 16 (4), 1478–1501. https://doi.org/10.1175/jhm-D-14-0155.1.

Beighley, R.E., Ray, R.L., He, Y., Lee, H., Schaller, L., Andreadis, K.M., Durand, M., Alsdorf, D.E., Shum, C.K., 2011. Comparing satellite derived precipitation datasets using the Hillslope River Routing (HRR) model in the Congo River Basin. Hydrol. Process. 25 (20), 3216–3229. https://doi.org/10.1002/hyp.8045.

Beven, K.J., 2006. A manifesto for the equifinality thesis. J. Hydrol. 320 (1–2), 18–36. https://doi.org/10.1016/j.jhydrol.2005.07.007.

Beven, K.J., 2012. Causal models as multiple working hypotheses about environmental processes. C.R. Geosci. 344 (2), 77–88. https://doi.org/10.1016/j.crte.2012.01.005.

Beven, K.J., Binley, A., 2014. GLUE: 20 years on. Hydrol. Process 28 (24), 5897–5918. https://doi.org/10.1002/hyp.10082.

Blazkova, S., Beven, K., 2009. A limits of acceptability approach to model evaluation and uncertainty estimation in flood frequency estimation by continuous simulation: skalka catchment, Czech Republic. Water Resour. Res. 45 (12), 1–12. https://doi.org/10.1029/2007WR006726.

Buchanan, B.P., Fleming, M., Schneider, R.L., Richards, B.K., Archibald, J., Qiu, Z., Walter, M.T., 2014. Evaluating topographic wetness indices across central New York agricultural landscapes. Hydrol. Earth Syst. Sci. 18, 3279–3299. https://doi.org/10.5194/hess-18-3279-2014.

Bultot, F., 1974. Atlas climatique du bassin zaïrois. Quatrième partie: pression atmosphérique, vent en surface et en altitude, température et humidité de l'air en altitude, nébulosité et visibilité, propriétés chimiques de l'air et des précipita- tions et classifications cl. Brussels I.N.E.A.C: 193 maps.

Chishugi, J.B., Alemaw, B.F., 2009. The Hydrology of the Congo River Basin: a GIS-based hydrological water balance model. In World Environmental and Water Resources Congress 2009 (pp. 1–16). 10.1061/41036(342)593.

Coxon, G., Freer, J., Westerberg, I.K., Wagener, T., Woods, R., Smith, P.J., 2015. A novel framework for discharge uncertainty quantification applied to 500 UK gauging stations. Water Resour. Res. 51, 2498–2514. https://doi.org/10.1002/2015WR017200.A.

Devroey, E.J., 1951. Observations Hydrographiques Au Congo belge Et Au Ruanda-Urundi. T.VI, 3 (1951-1959). Royal Academy for Overseas Sciences. https://www.kaowarsom.be/en/online_memoirs.

Döll, P., Fiedler, K., 2008. Global-scale modeling of groundwater recharge. Hydrol. Earth Syst. Sci. 12 (3), 863–885. https://doi.org/10.5194/hess-12-863-2008.

Ehlers, L.B., Sonnenborg, T.O., Heuvelink, G.B.M., He, X., Refsgaard, J.C., 2019. Joint treatment of point measurement, sampling and neighborhood uncertainty in space-time rainfall mapping. J. Hydrol. 574 (April), 148–159. https://doi.org/10.1016/j.jhydrol.2019.03.100.

Fekete, B.M., Vörösmarty, C.J., Grabs, W., 1999. Global, composite runoff fields based on observed river discharge and simulated water balances, Tech. Rep. 22. Global Runoff Data Cent., Koblenz, Germany.

Fleischmann, A., Siqueira, V., Paris, A., Collischonn, W., Paiva, R., Pontes, P., Crétaux, J., Bergé-Nguyen, M., Biancamaria, S., Gosset, M., Calmant, S., Tanimoun, B., 2018. Modelling hydrologic and hydrodynamic processes in basins with large semi-arid wetlands. J. Hydrol. 561 (August 2017), 943–959. https://doi.org/10.1016/j.jhydrol.2018.04.041.

Gupta, A., Govindaraju, R.S., 2019. Propagation of structural uncertainty in watershed hydrologic models. J. Hydrol. 575 (March), 66–81. https://doi.org/10.1016/j.jhydrol.2019.05.026.

Hansen, M.C., Roy, D.P., Lindquist, E., Adusei, B., Justice, C.O., Altstatt, A., 2008. A method for integrating MODIS and Landsat data for systematic monitoring of

forest cover and change in the Congo River Basin. Remote Sens. Environ. 112 (5), 2495–2513. https://doi.org/10.1016/j.rse.2007.11.012.
Harris, I., Jones, P.D., Osborn, T.J., Lister, D.H., 2014. Updated high-resolution grids of monthly climatic observations-the CRU TS3. 10 Dataset, 642 (May 2013), 623–642. 10.1002/joc.3711.
Her, Y., Seong, C., 2018. Responses of hydrological model equifinality, uncertainty, and performance to multi-objective parameter calibration. J. Hydroinf. 20 (4), 864–885. https://doi.org/10.2166/hydro.2018.108.
Horner, I., Renard, B., Le Coz, J., Branger, F., McMillan, H.K., Pierrefeu, G., 2018. Impact of stage measurement errors on streamflow uncertainty. Water Resour. Res. 54 (3), 1952–1976. https://doi.org/10.1002/2017WR022039.
Hrachowitz, M., Savenije, H.H.G., Blöschl, G., McDonnell, J.J., Sivapalan, M., Arheimer, B., Blume, T., Clark, M.P., Ehret, U., Fenicia, F., Freer, J.E., Gelfan, A., Gupta, H.V., Hughes, D.A., Hut, R.W., Montanari, A., Pande, S., Tetzlaff, D., Troch, P. A., Uhlenbrook, S., Wagener, T., Winsemius, H.C., Woods, R.A., Zehe, E., Cudennec, S., 2013. A decade of Predictions in Ungauged Basins (PUB) -a review. Hydrol. Sci. J. 58 (6), 1198–1255. https://doi.org/10.1080/02626667.2013.803183.
Hughes, D.A., 2013. A review of 40 years of hydrological science and practice in southern Africa using the Pitman rainfall-runoff model. J. Hydrol. 501, 111–124. https://doi.org/10.1016/j.jhydrol.2013.07.043.
Hughes, D.A., 2016. Hydrological modelling, process understanding and uncertainty in a Southern African context: lessons from the northern hemisphere. Hydrol. Process 30 (14), 2419–2431. https://doi.org/10.1002/hyp.10721.
Hughes, D.A., 2019. Facing a future water resources management crisis in sub-Saharan Africa. J. Hydrol. Reg. Stud. 23 (August 2018), 100600 https://doi.org/10.1016/j.ejrh.2019.100600.
Hughes, D.A., Andersson, L., Wilk, J., Savenije, H.H.G., 2006. Regional calibration of the Pitman model for the Okavango River. J. Hydrol. 331 (1–2), 30–42. https://doi.org/10.1016/j.jhydrol.2006.04.047.
Hughes, D.A., Farinosi, F., 2020. Assessing development and climate variability impacts on water resources in the Zambezi River basin. Simulating future scenarios of climate and development. J. Hydrol. Reg. Stud. 32 (December 2020), 100763 https://doi.org/10.1016/j.ejrh.2020.100763.
Hughes, D.A., Farinosi, F., 2021. Unpacking some of the linkages between uncertainties in observational data and the simulation of different hydrological processes using the Pitman model in data scarce Zambezi River basin. Hydrol. Process 35 (4), e14141. https://doi.org/10.1002/hyp.14141.
Hughes, D.A., Mazibuko, S., 2018. Simulating saturation-excess surface run-off in a semi-distributed hydrological model. Hydrol. Process. 32 (17), 2685–2694. https://doi.org/10.1002/hyp.13182.
Jung, H.C., Hamski, J., Durand, M., Alsdorf, D., Hossain, F., Lee, H., Hossain, A., Azad, K. M., Hasan, K., Khan, A.S., Hoque, A., Zeaul, K.M., 2010. Characterization of complex fluvial systems using remote sensing of spatial and temporal water level variations in the Amazon, Congo, and Brahmaputra Rivers. Earth Surf. Process. Landf. 34 (2010), 294–304. https://doi.org/10.1002/esp, 155–161304(February 2010).
Kabuya, P.M., Hughes, D.A., Tshimanga, R.M., Trigg, M.A., Bates, P., 2020b. Establishing uncertainty ranges of hydrologic indices across climate and physiographic regions of the Congo River Basin. J. Hydrol. Reg. Stud. 30 (August 2020), 100710 https://doi.org/10.1016/j.ejrh.2020.100710.
Kabuya, P.M., 2020. Constraining Simulation Uncertainties in a Hydrological Model of the Congo River Basin including a Combined Modelling Approach For Channel-Wetland Exchanges. Rhodes Univ., South Africa. PhD thesis. http://hdl.handle.net/10962/177997.
Kapangaziwiri, E., Hughes, D.A., Wagener, T., 2012. Incorporating uncertainty in hydrological predictions for gauged and ungauged basins in southern. Afr. Hydrol. Sci. J. 57 (5), 1000–1019. https://doi.org/10.1080/02626667.2012.690881.
Kiang, J.E., Gazoorian, C., Mcmillan, H., Coxon, G., Coz, J.Le., 2018. A Comparison of Methods for Stream Flow Uncertainty Estimation. Water Resour. Res. 54 (10), 7149–7176. https://doi.org/10.1029/2018WR022708.
Krause, P., Boyle, D.P., Bäse, F., 2005. Comparison of different efficiency criteria for hydrological model assessment. Adv. Geosci. 5, 89–97. https://hal.archives-ouvertes.fr/hal-00296842/document.
Laraque, A., Moukandi N'kaya, G.D., Orange, D., Tshimanga, R., Tshitenge, J.M., Mahé, G., Nguimalet, C.R., Trigg, M.A., Yopez, S., Gulemvuga, G., 2020. Recent Budget of Hydroclimatology and Hydrosedimentology of the Congo River in Central Africa. Water (Basel) 12 (9), 2613. https://doi.org/10.3390/w12092613.
Lempicka, M., 1971. Bilan hydrique du bassin du fleuve Zaïre. I: ecoulement du bassin 1950–1959. Office National de La Recherche et Du Développement. République Démocratique du Congo, Kinshasa.
Maidment, R.I., Allan, R.P., Black, E., 2015. Recent observed and simulated changes in precipitation over Africa. Geophys. Res. Lett. 42, 8155–8164. https://doi.org/10.1002/2015GL065765.
Mayaux, P., De Grandi, G., Malingreau, J.P., 2000. Central African forest cover revisited. Remote Sens. Environ. 71 (2), 183–196. https://doi.org/10.1016/s0034-4257(99)00073-5.
McMahon, T.A., Peel, M.C., 2019. Uncertainty in stage–discharge rating curves: application to Australian Hydrologic Reference Stations data. Hydrol. Sci. J. 64 (3), 255–275. https://doi.org/10.1080/02626667.2019.1577555.
McMillan, H., Krueger, T., Freer, J., 2012. Benchmarking observational uncertainties for hydrology: rainfall, river discharge and water quality. Hydrol. Process. 26, 4078–4111. https://doi.org/10.1002/hyp.9384, 2012.
McMillan, H., Seibert, J., Petersen-Overleir, A., Lang, M., White, P., Snelder, T., Rutherford, K., Krueger, T., Mason, R., Kiang, J., 2017. How uncertainty analysis of streamflow data can reduce costs and promote robust decisions in water management applications. Water Resour. Res. 53, 5220–5228. https://doi.org/10.1002/2015WR017200.
Mehdi, B., Schulz, K., Ludwig, R., Ferber, F., Lehner, B., 2018. Evaluating the importance of non-unique behavioural parameter sets on surface water quality variables under climate change conditions in a mesoscale agricultural watershed. Water Resour. Manag. 32 (2), 619–639. https://doi.org/10.1007/s11269-017-1830-3.
Moriasi, D.N., Arnold, J.G., Liew, M.W.Van, Bingner, R.L., Harmel, R.D., Veith, T.L., 2007. Model evaluation guidelines for systematic quantification of accuracy in watershed simulations. ASABE 50 (3), 885–900. https://pubag.nal.usda.gov/pubag/downloadPDF.xhtml?id=9298&content=PDF.
Munzimi, Y.A., Hansen, M.C., Asante, K.O., Munzimi, Y.A., Hansen, M.C., Asante, K.O., 2019. Estimating daily streamflow in the Congo Basin using satellite-derived data and a semi-distributed hydrological model. Hydrol. Sci. J. 64 (12), 1472–1487. https://doi.org/10.1080/02626667.2019.1647342.
Nash, J.E., Sutcliffe, J.V., 1970. River flow forecasting through conceptual models, Part 1-a discussion of principles. J. Hydrol. 10, 282–290. https://doi.org/10.1016/0022-1694(70)90255-6.
Ndzabandzaba, C., Hughes, D.A., 2017. Regional water resources assessments using an uncertain modelling approach: the example of Swaziland. J. Hydrol. Reg. Stud. 10, 47–60. https://doi.org/10.1016/j.ejrh.2017.01.002.
New, M., Lister, D., Hulme, M., Makin, I., 2002. A high-resolution data set of surface climate over global land areas. Clim. Res. 21 (1), 1–25. https://doi.org/10.3354/cr021001.
Nijzink, R.C., Almeida, S., Pechlivanidis, I.G., Capell, R., Gustafssons, D., Arheimer, B., Parajka, J., Freer, J., Han, D., Wagener, T., van Nooijen, R.R.P., Savenije, H.H.G., Hrachowitz, M., 2018. Constraining conceptual hydrological models with multiple information sources. Water Resour. Res. 54 (10), 8332–8362. https://doi.org/10.1029/2017WR021895.
Nilsson, C., Reidy, C.A., Dynesius, M., Revenga, C., 2005. Fragmentation and flow regulation of the world ' s Large River Systems. Science 308 (5720), 405–408. https://doi.org/10.1126/science.1107887.
O'Loughlin, F.E.O., Neal, J., Schumann, G.J.P., Beighley, E., Bates, P.D., 2019. A LISFLOOD-FP hydraulic model of the middle reach of the Congo. J. Hydrol. 580 (May), 124203 https://doi.org/10.1016/j.jhydrol.2019.124203.
Oosthuizen, N., Hughes, D.A., Kapangaziwiri, E., Kahinda, J.M., Mvandaba, V., 2018. Parameter and input data uncertainty estimation for the assessment of water resources in two sub-basins of the Limpopo River Basin. Proc. IAHS 378, 11–16. https://doi.org/10.5194/piahs-378-11-2018.
Pitman, W.V., 1973. A Mathematical Model For Generating Monthly River Flows from Meteorological Data in South Africa. Hydrological Research Unit, Univ. of Witwatersrand. Report No. 273.
Quesada-Montano, B., Westerberg, I.K., Fuentes-Andino, D., Hidalgo, H.G., Halldin, S., 2018. Can climate variability information constrain a hydrological model for an ungauged Costa Rican catchment? Hydrol. Process 32 (6), 830–846. https://doi.org/10.1002/hyp.11460.
Ruhoff, A.L., Paz, A.R., Aragao, L.E.O.C., Mu, Q., Malhi, Y., Collischonn, W., Rocha, H.R., Running, S.W., 2013. Assessment of the MODIS global evapotranspiration algorithm using eddy covariance measurements and hydrological modelling in the Rio Grande basin. Hydrol. Sci. J. 58 (8), 1658–1676. https://doi.org/10.1080/02626667.2013.837578.
Running, S., Mu, Q., Zhao, M., 2017. MOD16A2 MODIS/Terra Net Evapotranspiration 8-Day L4 Global 500 m SIN Grid V006 [Data set]. NASA EOSDIS Land Processes DAAC. Accessed 2021-06-14 from 10.5067/MODIS/MOD16A2.006.
Samba, G., Nganga, D., Mpounza, M., 2008. Rainfall and temperature variations over Congo-Brazzaville between 1950 and 1998. Theor. Appl. Climatol. 91 (1–4), 85–97. https://doi.org/10.1007/s00704-007-0298-0.
Santini, M., Caporaso, L., 2018. Evaluation of freshwater flow from rivers to the Sea in CMIP5 Simulations: insights from the Congo River Basin. J. Geophys. Res. Atmos 123 (18), 10. https://doi.org/10.1029/2017JD027422, 278-300.
Shafii, M., Tolson, B.A., 2015. Optimizing hydrological consistency by incorporating hydrological signatures into model calibration objectives. Water Resour. Res. 51, 3796–3814. https://doi.org/10.1002/2014WR016520.
Somorin, O.A., Brown, C.P.H., Visseren-Hamakers, I.J., Sonwa, D.J., Arts, B., Nkem, J., 2012. The Congo River Basin forests in a changing climate: policy discourses on adaptation and mitigation (REDD+). Glob. Environ. Change 22 (1), 288–298. https://doi.org/10.1016/j.gloenvcha.2011.08.001.
Sun, Q., Miao, C., Duan, Q., Ashouri, H., Sorooshian, S., Hsu, K.L., 2018. A review of global precipitation data sets: data sources, estimation, and inter- comparisons. Rev. Geophys. 56, 79–107. https://doi.org/10.1002/2017RG000574.
Teweldebrhan, A.T., Burkhart, J.F., Schuler, T.V., 2018. Parameter uncertainty analysis for an operational hydrological model using residual-based and limits of acceptability approaches. Hydrol. Earth Syst. Sci. 22 (9), 5021–5039. https://doi.org/10.5194/he-22-5021-2018.
Tshimanga, R.M., 2012. Hydrological Uncertainty Analysis and Scenario-based Streamflow Modelling for the Congo River Basin. Rhodes Univ., South Africa. PhD thesis. http://eprints.ru.ac.za/2937/.
Tshimanga, R.M., Hughes, D.A., 2014. Basin-scale performance of a semidistributed rainfall-runoff model for hydrological predictions and water resources assessment of large rivers: the Congo River. Water Resour. Res. 1174–1188. https://doi.org/10.1002/2013WR014310.
Tshimanga, R.M., Hughes, D.A., Kapangaziwiri, E., 2011. Initial calibration of a semi-distributed rainfall runoff model for the Congo River Basin. Phys. Chem. Earth 36 (14–15), 761–774. https://doi.org/10.1016/j.pce.2011.07.045.
Tshimanga, R., Bola, G., Kabuya, P., Nkaba, L., Neal, J., Trigg, M., Bates, P., Hughes, D., Laraque, A., Woods, R., Wagener, T., 2020. Towards a framework of catchment classification for hydrological predictions and water resources management in

ungauged basins of the Congo River. Chapman Congo Conference Monograph. AGU Books. https://doi.org/10.1002/essoar.10505549.1.
Tumbo, M., Hughes, D.A., 2015. Uncertain hydrological modelling: application of the Pitman model in the Great Ruaha River basin, Tanzania. Hydrol. Sci. J. Des Sci. Hydrol. 60 (11), 2047–2061. https://doi.org/10.1080/02626667.2015.1016948.
Velpuri, N.M., Senay, G.B., Singh, R.K., Bohms, S., Verdin, J.P., 2013. A comprehensive evaluation of two MODIS evapotranspiration products over the conterminous United States: using point and gridded FLUXNET and water balance ET. Remote Sens. Environ. 139, 35–49. https://doi.org/10.1016/j.rse.2013.07.013.
Waseem, M., Ajmal, M., Kim, T.W., 2016. Improving the flow duration curve predictability at ungauged sites using a constrained hydrologic regression technique. KSCE J. 20 (7), 3012–3021. https://doi.org/10.1007/s12205-016-0038-z.
Westerberg, I.K., Gong, L., Beven, K.J., Seibert, J., Semedo, A., Xu, C.Y., Halldin, S., 2014. Regional water balance modelling using flow-duration curves with observational uncertainties. Hydrol. Earth Syst. Sci. 18 (8), 2993–3013. https://doi.org/10.5194/hess-18-2993-2014.
Westerberg, I.K., Guerrero, J.L., Seibert, J., Beven, K.J., Halldin, S., 2011b. Stage-discharge uncertainty derived with a non-stationary rating curve in the Choluteca River, Honduras. Hydrol. Process 25 (4), 603–613. https://doi.org/10.1002/hyp.7848.
Westerberg, I.K., Guerrero, J.-.L., Younger, P.M., Beven, K.J., Seibert, J., Halldin, S., Freer, J.E., Xu, C.Y., 2011a. Calibration of hydrological models using flow duration curves. Hydrol. Earth Syst. Sci. 15 (7), 2205–2227. https://doi.org/10.5194/hess-15-2205-2011.
Westerberg, I.K., McMillan, H.K., 2015. Uncertainty in hydrological signatures. Hydrol. Earth Syst. Sci. 3951–3968. https://doi.org/10.5194/hess-19-3951-2015.
Wöhling, T., Samaniego, L., Kumar, R., 2013. Evaluating multiple performance criteria to calibrate the distributed hydrological model of the upper Neckar catchment. Environ. Earth Sci. 69, 453–468. https://doi.org/10.1007/s12665-013-2306-2.
Yadav, M., Wagener, T., Gupta, H., 2007. Regionalization of constraints on expected watershed response behavior for improved predictions in ungauged basins. Adv. Water Resour. 30 (8), 1756–1774. https://doi.org/10.1016/j.advwatres.2007.01.005.
Zeng, Z., Tang, G., Hong, Y., Zeng, C., Yang, Y., 2017. Development of an NRCS curve number global dataset using the latest geospatial remote sensing data for worldwide hydrologic applications. Remote Sens. Lett. 8 (6), 528–536. https://doi.org/10.1080/2150704X.2017.1297544.
Zhang, Z., Wagener, T., Reed, P., Bhushan, R., 2008. Reducing uncertainty in predictions in ungauged basins by combining hydrologic indices regionalization and multiobjective optimization. Water Resour. Res. 44 (12), 1–13. https://doi.org/10.1029/2008WR006833.